

Link persistence and conditional distances in multiplex networks

Fragkiskos Papadopoulos^{1,*} and Kaj-Kolja Kleineberg²

¹*Department of Electrical Engineering, Computer Engineering and Informatics,
Cyprus University of Technology, 33 Saripolou Street, 3036 Limassol, Cyprus*

²*Computational Social Science, ETH Zurich, Clausiusstrasse 50, 8092, Zurich, Switzerland*
(Dated: January 9, 2022)

Recent progress towards unraveling the hidden geometric organization of real multiplexes revealed significant correlations across the hyperbolic node coordinates in different network layers, which facilitated applications like trans-layer link prediction and mutual navigation. But are geometric correlations alone sufficient to explain the topological relation between the layers of real systems? Here we provide the negative answer to this question. We show that connections in real systems tend to persist from one layer to another irrespectively of their hyperbolic distances. This suggests that in addition to purely geometric aspects the explicit link formation process in one layer impacts the topology of other layers. Based on this finding, we present a simple modification to the recently developed Geometric Multiplex Model to account for this effect, and show that the extended model can reproduce the behavior observed in real systems. We also find that link persistence is significant in all considered multiplexes and can explain their layers' high edge overlap, which cannot be explained by coordinate correlations alone. Furthermore, by taking both link persistence and hyperbolic distance correlations into account we can improve trans-layer link prediction. These findings guide the development of multiplex embedding methods, suggesting that such methods should be accounting for both coordinate correlations and link persistence across layers.

I. INTRODUCTION

It has been shown that random geometric graphs in hyperbolic spaces are adequate models for complex networks, as they naturally and simultaneously possess many of their common structural and dynamical characteristics, including heterogeneous distributions of node degrees, strong clustering, and preferential attachment, cf. [1–9]. Specifically, the \mathbb{H}^2 model [1, 2] constructs networks by randomly distributing nodes on a hyperbolic disc of radius R , such that each node i has the polar coordinates, or hidden variables, r_i, θ_i , and connecting each pair of nodes with a probability that decreases with their hyperbolic distance.

Given the ability of the \mathbb{H}^2 model to construct synthetic networks that resemble real networks, it has been shown that one can meaningfully map (embed) real networks into the hyperbolic plane, in a way congruent with the model [10]. Mapped networks include the Autonomous Systems Internet [10], biological networks [11–13], social networks [3, 14], and the international trade system [15]. Using the constructed hyperbolic maps one can facilitate important applications, which include identifying node communities on a geometric basis [3, 10, 11, 16]; predicting missing and future links [11, 17, 18]; and performing efficient network navigation or search [10, 13, 17–21]. Model-free mapping methods have also been developed [22, 23].

The work in [3] explained the emergence of hyperbolic geometry by extending the static approach of [2] to growing networks. It has been shown that the radial coordinate of a node abstracts its *popularity*. The smaller

this coordinate, the more popular the node is, and the more likely it attracts connections. The angular distance between two nodes, i, j , $\Delta\theta_{ij}$, abstracts their *similarity*. The smaller this distance, the more similar the two nodes are, and the more likely they are connected. The hyperbolic distance between two nodes, very well approximated by $x_{ij} = r_i + r_j + 2 \ln \sin(\Delta\theta_{ij}/2)$ [2], is then a single-metric representation of a combination of the two attractiveness attributes, radial popularity and angular similarity.

The above framework has mainly focused on individual complex networks. In this view, given the connection probability function, the node coordinates alone determine the network's observed topology, and vice versa, the network's observed topology alone is used to infer its node coordinates. However, there are cases where nodes from one network may also exist in other networks. This gives rise to multiplex systems [24, 25], which are collections of networks (called layers) that share common nodes. Examples include the different social networks that a person may belong to [26, 27]; the Internet's IPv4 and IPv6 topologies [28]; structural and functional brain networks [29]; and networks of different types of genetic interactions [30]. This observation calls for extending the network geometry paradigm to the multiplex domain, where the different layers are treated simultaneously and not independently. This is because the coordinates and connections of nodes in one layer can, in principle, provide information about the coordinates and connections of the same nodes in other layers.

A first step towards this direction is the finding that if the layers comprising real multiplexes are independently embedded into hyperbolic spaces, their coordinates exhibit significant correlations [14]. This finding motivated new applications, like multidimensional community de-

* f.papadopoulos@cut.ac.cy

tection and trans-layer link prediction on a geometric basis, as well as multilayer greedy routing [14]. Furthermore, it was shown that the discovered correlations play an important role in the robustness of multiplexes against targeted attacks to high degree nodes [31] and to the outcome of evolutionary dynamics [32, 33]. Yet, despite these advances, it is still not fully understood to what extent can coordinate correlations alone explain the topological relation between the layers of real systems. In particular, are coordinate correlations alone sufficient to explain the high edge overlap observed among the layers of real systems [25, 34, 35]? This is an important metric as it has been shown to significantly affect the outcome of dynamical processes [36–38].

Here we provide the negative answer to the above question. We first provide empirical evidence from real multiplexes suggesting that connections can persist from one layer to another irrespectively of the hyperbolic distances that they span. We then consider a simple modification to the Geometric Multiplex Model (GMM) [14] to account for this effect, and show that the extended model can reproduce the behavior observed in real systems. We also estimate the link persistence probability in the considered systems and find that it is significant in all cases, explaining their layers' high edge overlap, which cannot be explained by coordinate correlations alone. Furthermore, we show that by taking link persistence into account one can improve trans-layer link prediction.

The rest of the paper is organized as follows. In Section II we review the \mathbb{H}^2 model, the GMM and the HyperMap embedding method [17, 18]. In Section III we provide empirical evidence of link persistence in real multiplexes. In Section IV we present the modified GMM and show that it reproduces the behavior observed in the real data. In Section V we show that link persistence explains the high edge overlap in real systems. In Section VI we analyze the model and explain how one can estimate the link persistence probability from the layers' hyperbolic embeddings. In Section VII we show that the accuracy of trans-layer link prediction can be improved by taking link persistence into account. Finally, in Section VIII we discuss open problems and conclude the paper.

II. PRELIMINARIES

In this section we review the \mathbb{H}^2 model [2], the GMM [14] and HyperMap [17, 18]. We limit ourselves only to the basic details that we will need in the rest of the paper. Throughout the paper, symbol ' \approx ' means *approximately equal*. Symbol ' \propto ' means *proportional to*, i.e., $f(t) \propto g(t)$ means $f(t) = cg(t)$, where c is a constant, $0 < c < \infty$. Sometimes there are additive terms so that $f(t) \propto g(t)$ can also mean $f(t) = cg(t) + d$.

A. \mathbb{H}^2 model

In the \mathbb{H}^2 model each node i has radial (popularity) and angular (similarity) coordinates r_i, θ_i . To construct a network that has size N , average node degree \bar{k} , a power law degree distribution with exponent $\gamma > 2$, and temperature $T \in [0, 1)$, we perform the following steps:

- (1) coordinate assignment: we sample the angular coordinates of nodes θ_i , $i = 1, 2, \dots, N$, uniformly at random from $[0, 2\pi]$, and their radial coordinates r_i , $i = 1, 2, \dots, N$, from the probability density function (PDF):

$$\rho(r) = \frac{1}{2\beta} \frac{\sinh \frac{r}{2\beta}}{\cosh \frac{R}{2\beta} - 1} \approx \frac{1}{2\beta} e^{\frac{1}{2\beta}(r-R)}, \quad (1)$$

where $\beta = \frac{1}{\gamma-1}$, while $R = 2 \ln \frac{N}{c}$ is the radius of the hyperbolic disc where nodes reside, and $c = \bar{k} \frac{\sin T\pi}{2T} \left(\frac{\gamma-2}{\gamma-1} \right)^2$;

- (2) creation of edges: we connect every pair of nodes i, j with the Fermi-Dirac connection probability:

$$p(x_{ij}) = \frac{1}{1 + e^{\frac{1}{2T}(x_{ij}-R)}}. \quad (2)$$

In the last expression, $x_{ij} \leq 2R$ is the hyperbolic distance between nodes i and j [39]:

$$\begin{aligned} x_{ij} &= \operatorname{arccosh}(\cosh r_i \cosh r_j - \sinh r_i \sinh r_j \cos \Delta\theta_{ij}) \\ &\approx r_i + r_j + 2 \ln \sin \frac{\Delta\theta_{ij}}{2} \approx r_i + r_j + 2 \ln \frac{\Delta\theta_{ij}}{2}, \end{aligned} \quad (3)$$

where $\Delta\theta_{ij} = \pi - |\pi - |\theta_i - \theta_j||$ is the angular distance between the nodes. The approximations in Eq. (3) hold for sufficiently large r_i, r_j , and $\Delta\theta_{ij} > 2\sqrt{e^{-2r_i} + e^{-2r_j}}$ [2]. Temperature T controls the average clustering [40] in the network, which is maximized at $T = 0$, and nearly linearly decreases to zero with $T \in [0, 1)$. At $T \rightarrow 0$ the connection probability in Eq. (2) becomes the step-function $p(x_{ij}) \rightarrow 1$ if $x_{ij} \leq R$, and $p(x_{ij}) \rightarrow 0$ if $x_{ij} > R$.

We also recall that the average degree of a node at radial coordinate r , $\bar{k}(r)$, is:

$$\bar{k}(r) \approx \bar{k}_0 e^{\frac{1}{2}(R-r)} \propto e^{-\frac{1}{2}r}, \quad (4)$$

where $\bar{k}_0 \equiv \bar{k}(\gamma - 2)/(\gamma - 1)$ is the expected minimum degree in the network. Therefore, $r(k) \propto 2 \ln(1/k)$. This combined with the fact that the density of radial coordinates increases exponentially, $\rho(r) \propto e^{\frac{1}{2\beta}r}$, gives the power law degree distribution, $P(k) \approx \rho(r(k))|r'(k)| \propto k^{-\gamma}$, $\gamma = 1 + 1/\beta > 2$. Without loss of generality, we assume here a hyperbolic plane of curvature $K = -1$. See [2] for further details.

B. Geometric Multiplex Model (GMM)

In the GMM each single layer is constructed according to the \mathbb{H}^2 model, while accounting for correlations among the radial and angular coordinates of nodes in the different layers, whose strength can be tuned. We overview here the GMM for two-layer systems, where each node $i \leq N$ exists in both layers. See [14] for the extension of the model to more than two layers and to layers with different sizes.

In a nutshell, we perform the following steps to construct a two-layer system:

- (1) assignment of coordinates $r_{1,i}, \theta_{1,i}$ to each node i in layer 1, as in the \mathbb{H}^2 model (Eqs. (6), (7) below);
- (2) assignment of coordinates $r_{2,i}, \theta_{2,i}$ to each node i in layer 2, depending on the node's coordinates in layer 1—the assignment here is done such that the marginal (unconditional) distribution of $r_{2,i}, \theta_{2,i}$ is still the one in the \mathbb{H}^2 model (Eqs. (8), (10));
- (3) creation of edges, by connecting node pairs in each layer with the corresponding \mathbb{H}^2 connection probability, which depends exclusively on the node coordinates in each layer (Eqs. (12), (13)).

Below, we explain these steps in more detail. To proceed, let:

$$\beta_i = \frac{1}{\gamma_i - 1}, R_i = 2 \ln \frac{N}{c_i}, c_i = \bar{k}_i \frac{\sin T_i \pi}{2T_i} \left(\frac{\gamma_i - 2}{\gamma_i - 1} \right)^2, \quad (5)$$

where \bar{k}_i , γ_i and T_i are respectively the target average degree, power law degree distribution exponent, and temperature in layer $i = 1, 2$.

(1) *Assignment of coordinates in layer 1.* For each node $i = 1, 2, \dots, N$ in layer 1 we sample its radial coordinate $r_{1,i}$ from the PDF:

$$\rho_1(r_1) = \frac{1}{2\beta_1} e^{\frac{1}{2\beta_1}(r_1 - R_1)}, \quad (6)$$

while its angular coordinate $\theta_{1,i}$ is sampled from the uniform PDF:

$$f(\theta) = \frac{1}{2\pi}, \quad \theta \in [0, 2\pi]. \quad (7)$$

(2) *Assignment of coordinates in layer 2.* The radial coordinate $r_{2,i}$ of each node $i = 1, 2, \dots, N$ in layer 2 is sampled from the conditional PDF:

$$\begin{aligned} \rho_2(r_2 | r_1 = r_{1,i}, \eta) &= \frac{1}{2\beta_2} e^{\phi_1 - (\phi_1^\eta + \phi_2^\eta)^{\frac{1}{\eta}}} (\phi_1 \phi_2)^{\eta-1} \\ &\times (\phi_1^\eta + \phi_2^\eta)^{\frac{1}{\eta}-2} \left((\phi_1^\eta + \phi_2^\eta)^{\frac{1}{\eta}} + \eta - 1 \right), \quad (8) \\ \phi_i &\equiv \frac{R_i - r_i}{2\beta_i}, \quad i = 1, 2, \quad \eta \equiv \frac{1}{1 - \nu} \in [1, \infty), \end{aligned}$$

where $\nu \in [0, 1)$ is the radial correlation strength parameter. The higher the value of ν the stronger is the

correlation between $r_{2,i}$ and $r_{1,i}$. At $\nu \rightarrow 1$, $r_{1,i}, r_{2,i}$ are maximally correlated, while at $\nu = 0$, $r_{1,i}, r_{2,i}$ are uncorrelated. We note that $r_{1,i} = r_{2,i}$ at $\nu \rightarrow 1$ only if $R_1 = R_2$ and $\beta_1 = \beta_2$. To derive Eq. (8) we use the bivariate Gumbel-Hougaard copula [14], see Appendix B. The copula ensures that no matter the value of ν the marginal PDF of $r_{2,i}$ is the same as in the \mathbb{H}^2 model:

$$\rho_2(r_2) = \frac{1}{2\beta_2} e^{\frac{1}{2\beta_2}(r_2 - R_2)}. \quad (9)$$

The angular coordinate $\theta_{2,i}$ of each node $i = 1, 2, \dots, N$ in layer 2 is obtained by:

$$\theta_{2,i} = \text{mod} \left[\theta_{1,i} + \frac{2\pi l_i}{N}, 2\pi \right], \quad (10)$$

where l_i is a directed arc length on the circle of radius $R = N/(2\pi)$, sampled from the zero-mean truncated Gaussian PDF:

$$\begin{aligned} f_g(l) &= \frac{\phi\left(\frac{l}{\sigma}\right)}{\sigma \text{erf}\left(\frac{N}{2\sqrt{2}\sigma}\right)}, \quad (11) \\ -\frac{N}{2} \leq l \leq \frac{N}{2}, \quad \sigma &\equiv \sigma_0 \left(\frac{1}{g} - 1 \right), \end{aligned}$$

where $\sigma \in [0, \infty)$ is the standard deviation of the PDF, while $g \in (0, 1]$ is the angular correlation strength parameter. Furthermore, $\sigma_0 = \min[100, N/(4\pi)]$ denotes the standard deviation for $g = 0.5$, $\phi(x) = \frac{1}{\sqrt{2\pi}} e^{-\frac{1}{2}x^2}$, and $\text{erf}(x) = \frac{2}{\sqrt{\pi}} \int_0^x e^{-t^2} dt$ is the Gauss error function.

The higher the value of g the stronger is the correlation between $\theta_{2,i}$ and $\theta_{1,i}$. At $g \rightarrow 0$, $\sigma \rightarrow \infty$, $f_g(l)$ becomes the uniform PDF, and $\theta_{2,i}, \theta_{1,i}$ are uncorrelated. At $g = 1$, $\sigma = 0$, and $l_i = 0$, meaning that the angles of each node are the same in the two layers. The marginal PDF of $\theta_{2,i}$ is still the uniform PDF (Eq. (7)).

(3) *Creation of edges.* Once all node coordinates are assigned, we connect each node pair i, j in layers 1 and 2 with the corresponding \mathbb{H}^2 connection probabilities given in Eqs. (12), (13) below:

$$p_1(x_1^{ij}) = \frac{1}{1 + e^{\frac{1}{2T_1}(x_1^{ij} - R_1)}}, \quad (12)$$

$$p_2(x_2^{ij}) = \frac{1}{1 + e^{\frac{1}{2T_2}(x_2^{ij} - R_2)}}, \quad (13)$$

where $x_1^{ij} \leq 2R_1, x_2^{ij} \leq 2R_2$ are the hyperbolic distances between nodes i, j in layers 1 and 2.

C. HyperMap

Finally, given a real network, the HyperMap method [17, 18] can be used to infer the popularity and similarity coordinates of its nodes. The method is based on maximum likelihood estimation. On its input it takes the network adjacency matrix α_{ij} ($\alpha_{ij} = \alpha_{ji} = 1$ if there

is a link between nodes i and j , and $\alpha_{ij} = \alpha_{ji} = 0$ otherwise), and computes radial and angular coordinates r_i, θ_i , for all nodes $i \leq N$. The radial coordinates are related to the observed node degrees k_i :

$$r_i \propto R - 2 \ln k_i, \quad (14)$$

while the angular coordinates are found by maximizing the likelihood:

$$\mathcal{L} = \prod_{1 \leq j < i \leq N} p(x_{ij})^{\alpha_{ij}} [1 - p(x_{ij})]^{1 - \alpha_{ij}}. \quad (15)$$

The product in the above relation goes over all node pairs i, j in the network, x_{ij} is the hyperbolic distance between pair i, j and $p(x_{ij})$ is the connection probability in Eq. (2). HyperMap was used in [14] to independently map the layers of different real multiplexes into hyperbolic spaces. Its implementation is available at [41].

III. EVIDENCE OF LINK PERSISTENCE IN REAL MULTIPLEXES

We now provide empirical evidence from real multiplexes suggesting that connections can persist from one layer to another irrespectively of the hyperbolic distances that they span. We call such links *persistent links*. To this end, we consider layer pairs of different real multiplexes and their hyperbolic embeddings from [14]. See Table I for an overview of the data and Appendix A for further details. The correlation strengths ν, g in Table I were estimated in [14]. The considered multiplexes are paradigmatic systems from different domains: technological (Internet), biological (Drosophila, C. Elegans, Human Brain), scientific collaboration (arXiv), and society (Physicians). We have verified that similar results hold in the other multiplexes and layer pairs considered in [14].

Let us classify all pairs of nodes in layer 1 that also exist in layer 2 into three sets. First, S_c contains the pairs connected in layer 1. Second, S_d contains the pairs disconnected in layer 1. Finally, S_{all} simply contains all pairs in S_c and S_d . For each set, we compute the empirical trans-layer connection probability, which is the probability that a pair in the set is connected in layer 2 given its hyperbolic distance x_1 in layer 1. These probabilities are respectively denoted by $p_{trans}^c(x_1)$, $p_{trans}^d(x_1)$, $p_{trans}^{all}(x_1)$, and computed as follows. For each set, we compute the hyperbolic distances among its pairs in layer 1. We then bin the range of hyperbolic distances from zero to the maximum distance into small bins. For each bin we find all the pairs located at the hyperbolic distances falling within the bin. The percentage of pairs in this set of pairs that are connected in layer 2 is the value of the corresponding trans-layer connection probability at the bin.

For each of S_c, S_d, S_{all} , we also compute the empirical connection probability in layer 2, $p_2^c(x_2)$, $p_2^d(x_2)$, $p_2^{all}(x_2)$.

These probabilities are computed following the same binning procedure as above, except that we consider the hyperbolic distances x_2 among the pairs in layer 2 instead of layer 1. For each of S_c, S_d, S_{all} , we further compute the average hyperbolic distance among its pairs in layer 2 conditioned on their distance in layer 1, $E^c[x_2|x_1]$, $E^d[x_2|x_1]$, $E^{all}[x_2|x_1]$. This metric is used to illustrate the hyperbolic distance correlations for each set of nodes in the two layers.

The results are shown in Fig. 1, where we make similar observations in all considered multiplexes.¹ First, we see that $p_{trans}^{all}(x_1)$ decreases with x_1 . This means that nodes at smaller hyperbolic distances in layer 1 have higher chances of being connected in layer 2, as already observed [14]. However, here we also observe that $p_{trans}^c(x_1)$ is significantly larger than $p_{trans}^d(x_1)$, and virtually independent of x_1 at $x_1 > R_2$. Furthermore, even though it may have an increasing trend at $x_1 < R_2$, it does not drastically change. These observations suggest that a significant percentage of connected layer 1 pairs remain connected in layer 2 irrespectively of their distances x_1 ; and consequently, irrespectively of their distances x_2 . We also see that at smaller x_1 , $p_{trans}^c(x_1) = p_{trans}^{all}(x_1)$. This is because there are no disconnected pairs at those distances, i.e., $S_c = S_{all}, S_d = \emptyset$ for those distances. At larger x_1 , where $S_d \neq \emptyset$, we see that $p_{trans}^d(x_1)$ decreases with x_1 , similarly to $p_{trans}^{all}(x_1)$.

The empirical connection probabilities $p_2^c(x_2)$, $p_2^d(x_2)$, $p_2^{all}(x_2)$ also show that at large $x_2 > R_2$ the connected layer 1 pairs have significantly higher chances of being connected in layer 2, compared to the disconnected layer 1 pairs. On the other hand, at smaller $x_2 < R_2$ both sets of pairs have similarly high chances of being connected.

Based on the above observations in the next section we consider a simple modification to the GMM, where a percentage of connected pairs in layer 1 remain connected in layer 2 irrespectively of their distances, and show that the modified GMM reproduces the behavior observed in Fig. 1.

IV. GMM WITH LINK PERSISTENCE (GMM-LP)

To construct a two-layer synthetic multiplex with the modified GMM (GMM-LP) we follow exactly the same steps as in the GMM (Sec. IIB), except that nodes in layer 2 connect according to the following procedure:

- (1) if the nodes are connected in layer 1, they remain connected in layer 2 with probability w or connect according to Eq. (13);

¹ Similar results hold if we consider the layers in the direction 2 to 1 instead of 1 to 2 (see Sec. VI E for the estimated link persistence probabilities in the direction 2 to 1).

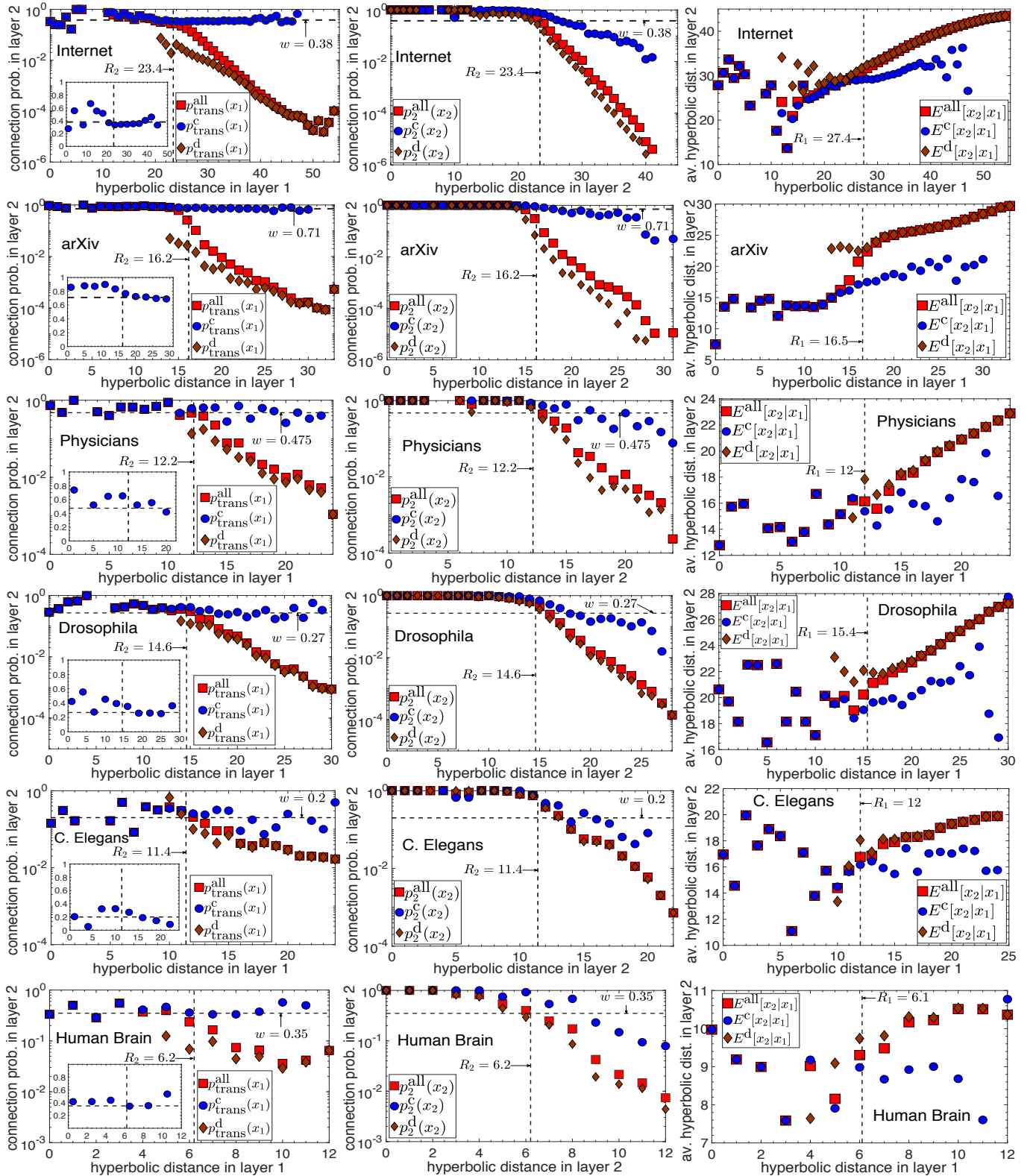


FIG. 1. Link persistence and hyperbolic distance correlations in the IPv4/IPv6 Internet, arXiv, Physicians, Drosophila, C. Elegans and Human Brain multiplexes. The plots show the trans-layer connection probabilities $p_{\text{trans}}^{\text{all}}(x_1)$, $p_{\text{trans}}^c(x_1)$, $p_{\text{trans}}^d(x_1)$, the connection probabilities $p_2^{\text{all}}(x_2)$, $p_2^c(x_2)$, $p_2^d(x_2)$, and the conditional average hyperbolic distances $E^{\text{all}}[x_2|x_1]$, $E^c[x_2|x_1]$, $E^d[x_2|x_1]$. The y -axes in the connection probability plots are in log-scale. The insets show $p_{\text{trans}}^c(x_1)$ in linear scale. The bins in the x -axes have size 1 except from the insets where larger bins have been used to reduce fluctuations. The horizontal dashed lines indicate the value of the estimated link persistence probability w (Sec. VI E). The vertical dashed lines indicate the hyperbolic disc radii R_1, R_2 of layers 1 and 2.

Name	Type	Nodes	layer 1, layer 2	ν, g
Internet	Technological	Autonomous Systems	IPv4 AS topology, IPv6 AS topology	0.40, 0.40
Drosophila	Biological	Proteins	Suppressive genetic interaction, additive genetic interaction	0.47, 0.82
C. Elegans	Biological	Neurons	Electric, chemical monadic synaptic junctions	0.22, 0.48
Human Brain	Biological	Brain regions	Structural network, functional network	0.18, 0.42
arXiv	Collaboration	Authors	cond-mat.disnn and physics.bioph categories	0.45, 0.93
Physicians	Social	Physicians	Discussion, advise relations	0.47, 0.84

TABLE I. Overview of the considered real-world multiplex network data.

- (2) if the nodes are disconnected in layer 1, or exist only in layer 2, they connect according to Eq. (13).

We call $w \in [0, 1]$ *link persistence probability*. In other words, the connection probability among connected layer 1 pairs in layer 2 is:

$$\begin{aligned} p_2^c(x_2) &= w + (1 - w)p_2(x_2) \\ &= p_2(x_2) + (1 - p_2(x_2))w, \end{aligned} \quad (16)$$

while for the disconnected layer 1 pairs:

$$p_2^d(x_2) = p_2(x_2). \quad (17)$$

We can see from Eqs. (16), (17) that the considered modification is equivalent to the following simpler procedure that we implement in the GMM-LP²:

- (1) construct layers 1 and 2 using the GMM;
- (2) select at random a percentage w of connected pairs in layer 1 that also exist in layer 2;
- (3) connect the selected pairs in layer 2 if they are not already connected.

Fig. 2 shows the trans-layer connection probabilities $p_{\text{trans}}^{\text{all}}(x_1)$, $p_{\text{trans}}^c(x_1)$, $p_{\text{trans}}^d(x_1)$ and the connection probabilities $p_2^{\text{all}}(x_2)$, $p_2^c(x_2)$, $p_2^d(x_2)$ in synthetic versions of the Internet, arXiv, Physicians, Drosophila, C. Elegans and Human Brain multiplexes constructed using the GMM-LP. Fig. 3 also shows the corresponding average hyperbolic distances $E^{\text{all}}[x_2|x_1]$, $E^c[x_2|x_1]$, $E^d[x_2|x_1]$. Each synthetic layer $i = 1, 2$ has approximately the same number of nodes N_i , average degree, power law degree distribution exponent γ_i and temperature T_i as the corresponding real layer, see Appendix A for the values of these parameters. For simplicity, in these synthetic systems all nodes in the smaller layer also exist in the larger, while the corresponding correlation strengths ν, g and link persistence probabilities w are the ones shown in Table I and Fig. 1.

For each synthetic multiplex, Figs. 2, 3 show the results with the real node coordinates, as well as with the

inferred node coordinates that are obtained after independently mapping each layer to its hyperbolic space using HyperMap. The reason of performing the latter is to facilitate a more direct comparison with the plots of Fig. 1 where the layers are also embedded independently. We observe that the resemblance of Figs. 2, 3 with Fig. 1 is remarkable, especially for the embedded synthetic layers. We note that by maximizing the likelihood in Eq. (15) connected nodes are attracted and placed closer to each other in the hyperbolic space while disconnected nodes repel. This explains why in general $E^c[x_2|x_1] < E^d[x_2|x_1]$ in the embeddings. This effect can also impose a decreasing trend in $p_2^c(x_2)$ at large $x_2 > R_2$ (also observed in Fig. 1), which does not exist if the real coordinates are used and where we can clearly see that $p_2^c(x_2) \approx w$ (Fig. 2). $p_{\text{trans}}^c(x_1)$ appears less prone to embedding effects and we can see in Fig. 2 that $p_{\text{trans}}^c(x_1) \approx w$ at $x_1 > R_2$, as in the real systems (Fig. 1).

Taken altogether, the GMM-LP can capture the behavior observed in real systems remarkably well. In Section VI we analyze the model and prove the behavior observed in Fig. 2. Furthermore, we show that the main topological properties of layer 2 in GMM-LP are very similar to the ones in GMM. Below, we show that link persistence drives the high edge overlap observed in real systems.

V. LINK PERSISTENCE AND EDGE OVERLAP

The edge overlap O between two layers (layer 1, layer 2) is formally defined as the ratio of the number of overlapping (i.e., common) edges between the layers, to the maximum possible number of common edges [34]:

$$O = \frac{\#(\text{overlapping edges})}{\min[\#(\text{edges in layer 1}), \#(\text{edges in layer 2})]}, \quad (18)$$

where the number of edges in each layer in the denominator is computed only among the common nodes.

Fig. 4(a) shows the edge overlap O in the real systems of Fig. 1 and in their synthetic counterparts of Figs. 2, 3. The figure also shows the overlap in synthetic systems constructed with the same parameters and correlation strengths as the ones of Figs. 2, 3 but without link persistence ($w = 0$). We see that the synthetic systems with link persistence exhibit a high edge overlap similar to

² The code implementing GMM-LP can be found online at [42].

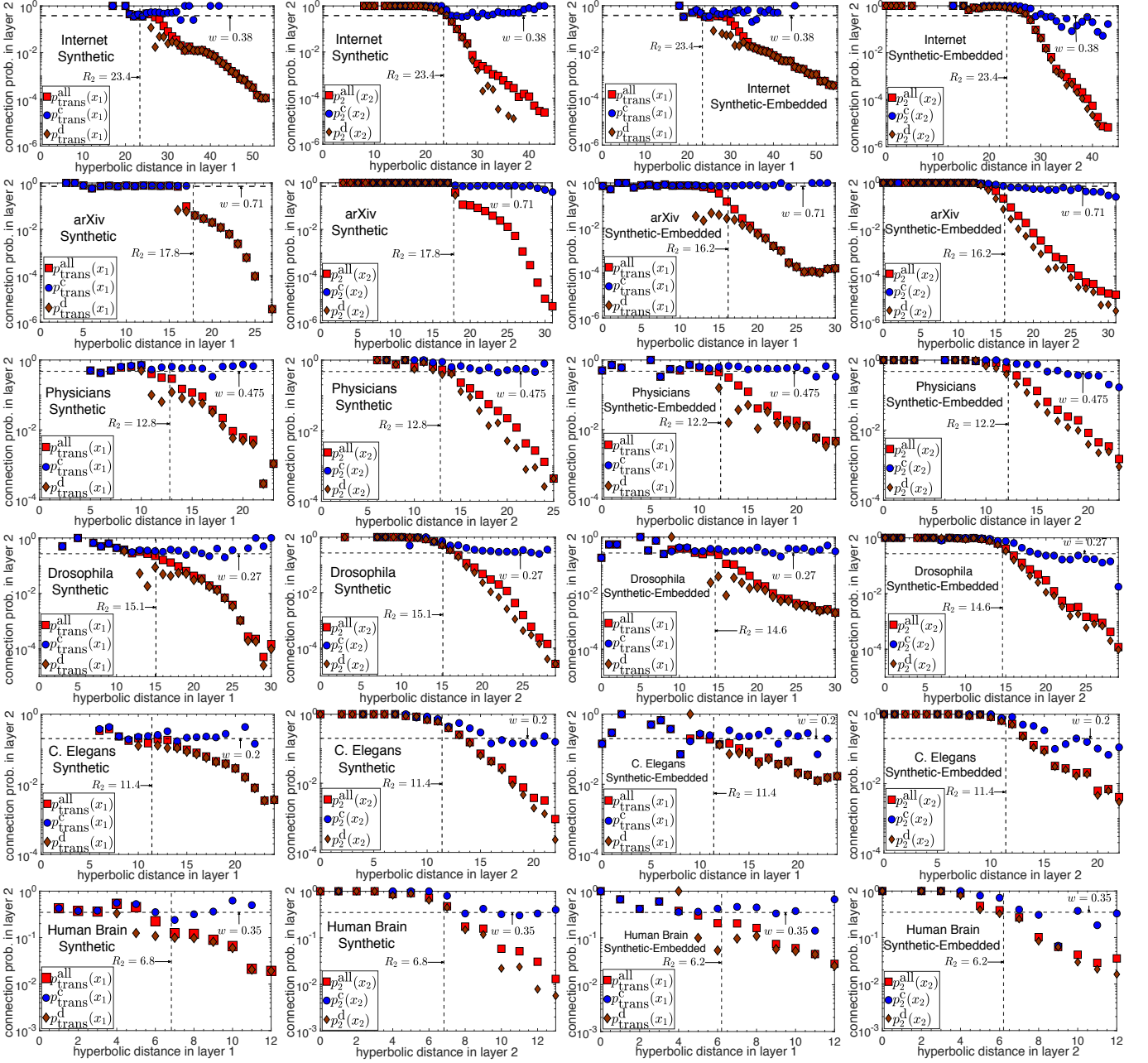


FIG. 2. Link persistence in synthetic versions of the multiplexes in Fig. 1 constructed using the GMM-LP. The plots show the trans-layer connection probabilities between layers 1 and 2 and the connection probabilities in layer 2, as in Fig. 1. The first two columns are the results with the real node coordinates, while the next two columns are the results with the inferred node coordinates.

the real systems, while the ones without link persistence have a significantly lower overlap. To achieve the same overlap in synthetic systems without link persistence we need significantly higher correlation strengths than those in Table I. For example, in the synthetic versions of the Human Brain, C. Elegans and Internet multiplexes we would need $\nu = g \approx 0.7$, $\nu = g \approx 0.8$, $\nu = g \approx 0.9$, respectively, while in Drosophila, Physicians and arXiv we cannot achieve the same overlap as in the real systems

even with $\nu = g \approx 1$. Fig. 4(b) shows that the edge overlap in the considered systems is very well correlated with their estimated link persistence probabilities w (horizontal dashed lines in Fig. 1), further highlighting that link persistence is the driving force for their observed high edge overlap.

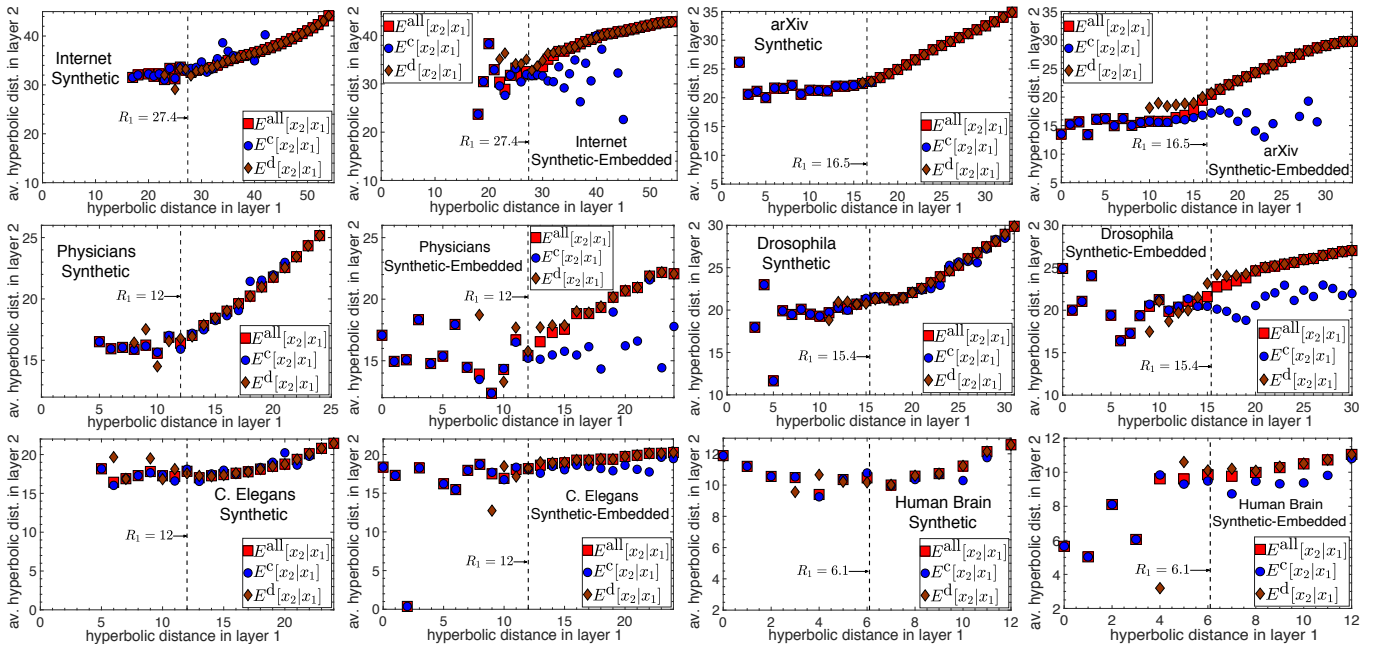


FIG. 3. Hyperbolic distance correlations in synthetic versions of the multiplexes in Fig. 1 constructed using the GMM-LP. The plots show the conditional average hyperbolic distances as in Fig. 1. For each multiplex the first plot are the results with the real node coordinates while the second plot are the results with the inferred node coordinates.

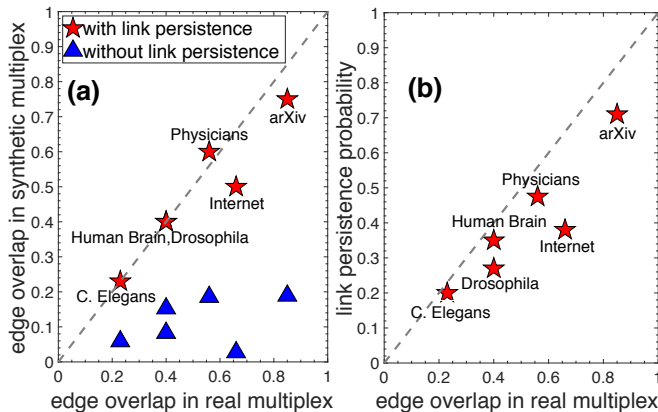


FIG. 4. (a) Edge overlap O in real systems vs. synthetic counterparts with and without link persistence. (b) Edge overlap O in real systems vs. link persistence probability w .

VI. ANALYSIS OF THE GMM-LP

In this section we analyze the GMM-LP. We first analyze the connection probabilities in layer 2, $p_2^c(x_2)$, $p_2^d(x_2)$, $p_2^{\text{all}}(x_2)$, and investigate the layer's degree distribution and clustering. We then analyze the trans-layer connection probabilities $p_{\text{trans}}^c(x_1)$, $p_{\text{trans}}^d(x_1)$, $p_{\text{trans}}^{\text{all}}(x_1)$, which will inform us of how we can improve trans-layer link prediction by taking link persistence into account.

A. Connection probabilities in layer 2

The connection probabilities among connected and disconnected layer 1 pairs in layer 2 are given by Eqs. (16), (17). At $x_2 \gg R_2 - 2T_2 \ln w$, $p_2^c(x_2) \approx (1 - p_2(x_2))w \approx w$, while at $x_2 \ll R_2 - 2T_2 \ln w$, $p_2^c(x_2) \approx p_2(x_2) = p_2^d(x_2)$, justifying the observed behavior in Fig. 2. Below, we analyze $p_2^{\text{all}}(x_2)$. Since link persistence is relevant only among common pairs, to ease exposition we assume that the two layers consist of N common nodes.

Let $f_1(x_1)$, $f_2(x_2)$ be the PDFs of the hyperbolic distances x_1, x_2 among pairs in layers 1 and 2. Further, let $f(x_1|x_2)$ be the PDF of the hyperbolic distance x_1 of a pair in layer 1, conditioned on its distance x_2 in layer 2. Even though the PDFs admit closed-form expressions [43], the conditional PDF depends on the radial and angular correlation strengths ν, g and does not have an analytic expression (see Appendix D). Nevertheless, we can still deduce the behavior of $p_2^{\text{all}}(x_2)$.

Let $\eta(x_2)$ be the probability that a pair of nodes at distance x_2 is connected in layer 1:

$$\eta(x_2) = \int_0^{2R_1} f(x_1|x_2)p_1(x_1)dx_1, \quad (19)$$

where $p_1(x_1)$ is the connection probability in layer 1 (Eq. (12)). If there are distance correlations, $\eta(x_2)$ decreases with x_2 since $f(x_1|x_2)$ concentrates over higher x_1 values and $p_1(x_1)$ decreases with x_1 . The stronger the correlations, the faster $\eta(x_2)$ decreases with x_2 as x_1 is

more narrowly distributed around x_2 . If there are no correlations, $f(x_1|x_2) = f_1(x_1)$, and $\eta(x_2)$ is the constant:

$$\eta(x_2) \equiv \eta = \frac{\bar{k}_1}{N}, \quad (20)$$

where \bar{k}_1 is the average degree in layer 1. On the other hand, in the maximally correlated case where nodes coordinates are identical in the two layers,³ $f(x_1|x_2) = \delta(x_1 - x_2)$, where δ is the Dirac delta function, and:

$$\eta(x_2) = p_1(x_2). \quad (21)$$

Using Eqs. (16), (17), (19) we can write:

$$\begin{aligned} p_2^{\text{all}}(x_2) &= \eta(x_2)p_2^c(x_2) + (1 - \eta(x_2))p_2^d(x_2) \\ &= p_2(x_2) + (1 - p_2(x_2))w\eta(x_2). \end{aligned} \quad (22)$$

Therefore, $p_2^{\text{all}}(x_2)$ differs from the connection probability in the \mathbb{H}^2 model, $p_2(x_2)$, by the term $(1 - p_2(x_2))w\eta(x_2)$. The term $1 - p_2(x_2)$ is the percentage of disconnected pairs at distance x_2 in the \mathbb{H}^2 model, while $w\eta(x_2)$ is the percentage of these pairs that are connected by a persistent link in GMM-LP. At $x_2 \gg R_2$, $(1 - p_2(x_2))w\eta(x_2) \approx w\eta(x_2)$ and $p_2^{\text{all}}(x_2) \approx p_2(x_2) + w\eta(x_2)$. At $x_2 \ll R_2$, $p_2^{\text{all}}(x_2) \approx p_2(x_2)$.

We thus see that persistent links affect the connection probability mostly at large distances $x_2 \gg R_2$, increasing its tail. This is validated in Fig. 5(a) where we also see that the stronger the correlations the faster the connection probability decreases at large distances. In other words, with stronger correlations pairs at smaller distances have higher chances of being connected by a persistent link, as expected, and as also seen in Fig. 5(b). Since persistent links increase the connection probability at large distances, they decrease the average clustering in the network, akin to increasing the temperature in the \mathbb{H}^2 model (Sec. II A). This is seen in Fig. 5(c), where we also see that the stronger the correlations the smaller the decrease is, as also expected, since shorter distance connections are preferred. Below, we show that the tail of the degree distribution remains the same as in the \mathbb{H}^2 model, irrespectively of the correlation strengths (Fig. 5(d)).

B. Degree distribution in layer 2

We first recall that in the \mathbb{H}^2 model the average degree of a node decreases exponentially with its radial coordinate r , $\bar{k}(r) \propto e^{-\frac{1}{2}r}$ (Eq. (4)), while the density of radial coordinates increases exponentially, $\rho(r) \propto e^{\frac{1}{2\beta}r}$. The combination of these two exponentials gives a power law degree distribution, $P(k) \propto k^{-\gamma}$, $\gamma = 1 + 1/\beta > 2$.

³ Angular coordinates are identical at $g = 1$ (Eqs. (10), (11)), while radial coordinates are identical at $\nu \rightarrow 1$ if $\gamma_1 = \gamma_2$ and $\bar{k}_1/\bar{k}_2 = T_1 \sin T_2\pi / (T_2 \sin T_1\pi)$ (Eqs. (8), (5)).

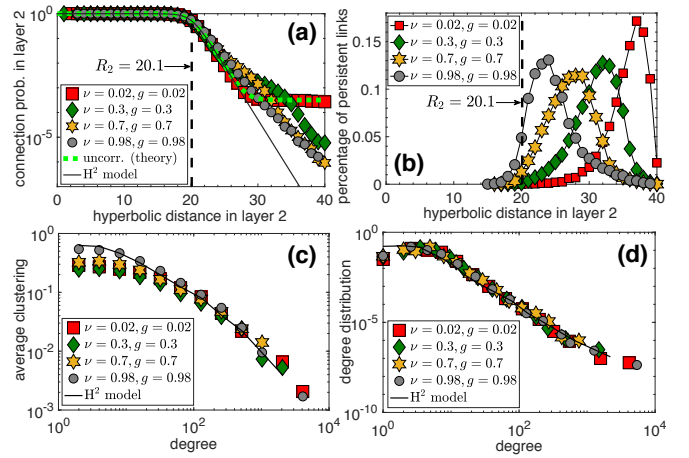


FIG. 5. (a) Connection probability $p_2^{\text{all}}(x_2)$. (b) Distribution of persistent links over the hyperbolic distances in layer 2. (c) Degree-depended average clustering $\bar{c}(k)$. (d) Degree distribution $P(k)$. The results correspond to layer 2 of a two-layer synthetic multiplex with $N = 10^4$ nodes, $\gamma_1 = 2.8, \gamma_2 = 2.3, T_1 = 0.7, T_2 = 0.5, \bar{k}_1 = \bar{k}_2 = 8$, link persistence probability $w = 0.4$ and correlation strengths as shown in the legends. In (a) the green dotted line is the theoretical prediction for the uncorrelated case ($\eta(x_2)$ given by Eq. (20)), while the solid line is the connection probability in the \mathbb{H}^2 model (Eq. (13)). In (a), (b) the vertical dashed lines indicate the hyperbolic disc radius R_2 . In (c), (d) the solid lines are the corresponding results in a synthetic network constructed with the \mathbb{H}^2 model with the same parameters as layer 2.

In our case the density of radial coordinates is the same as in the \mathbb{H}^2 model. Therefore, to investigate the degree distribution we analyze $\tilde{k}_2(r)$, which is the average degree of a node with radial coordinate r in layer 2, to see whether it still decreases as $e^{-\frac{1}{2}r}$. Since the hyperbolic distance x between two nodes is a function of their radial coordinates r, r' and angular distance $\Delta\theta$ (Eq. (3)), $p_2^{\text{all}}(x)$ is a function of $r, r', \Delta\theta$, and we can write:

$$\tilde{k}_2(r) = \frac{N}{\pi} \int_0^{R_2} \rho_2(r') dr' \int_0^\pi p_2^{\text{all}}(r, r', \Delta\theta) d\Delta\theta. \quad (23)$$

The above relation does not have a closed-form expression except in the uncorrelated and maximally correlated cases (Eqs. (20), (21)), with the additional requirement in the latter that the temperatures of the two layers are the same, $T_1 = T_2$. In the uncorrelated case we have (see Appendix C):

$$\tilde{k}_2(r) \approx \left(1 - \frac{w\bar{k}_1}{N}\right) \bar{k}_2(r) + w\bar{k}_1, \quad (24)$$

where:

$$\bar{k}_2(r) \equiv \bar{k}_{0,2} e^{\frac{1}{2}(R_2 - r)}, \quad \bar{k}_{0,2} \equiv \bar{k}_2 \left(\frac{\gamma_2 - 2}{\gamma_2 - 1} \right). \quad (25)$$

We can see from the above relations that $\tilde{k}_2(r) \approx \bar{k}_2(r)$

for large N and $r \ll R_2 - 2 \ln(w\bar{k}_1/\bar{k}_{0,2}) \propto \ln N$.⁴

In the maximally correlated case we can show (Appendix C) that:

$$A\bar{k}_2(r) \leq \tilde{\tilde{k}}_2(r) \leq B\bar{k}_2(r), \quad (26)$$

where $A \equiv (1 + wC - w\sqrt{C(1-T_1)(1-T_2)})$, $B \equiv (1 + wC)$, $C \equiv T_1 \sin T_2 \pi / (T_2 \sin T_1 \pi)$, and $\bar{k}_2(r)$ in Eq. (25). Therefore $\tilde{\tilde{k}}_2(r) \propto \bar{k}_2(r)$. If in addition $T_1 = T_2$:

$$\tilde{\tilde{k}}_2(r) \approx (1 + wT_2)\bar{k}_2(r). \quad (27)$$

Our analysis shows that if there are no distance correlations $\tilde{\tilde{k}}_2(r) \propto e^{-\frac{1}{2}r}$ for sufficiently small r . Small values of r correspond to higher expected degrees and hence the degree distribution still scales as $P(k) \propto k^{-\gamma_2}$, $\gamma_2 = 1 + 1/\beta_2 > 2$. This result is expected since persistent links randomly connect pairs at larger distances (cf. Fig. 5(a)), which correspond primarily to low degree nodes. As distance correlations increase, persistent links tend to connect pairs at smaller distances (Fig. 5(b)), which results in more connections to higher degree nodes, see Fig. 6. At strongest correlations, we see from Eq. (26) that $\tilde{\tilde{k}}_2(r) \propto \bar{k}_2(r) \forall r$, meaning again that $P(k) \propto k^{-\gamma_2}$. We can thus conclude that no matter the correlation strengths, persistent links do not affect the tail of the degree distribution, which remains the same as in the \mathbb{H}^2 model. This result is validated in Fig. 5(d).

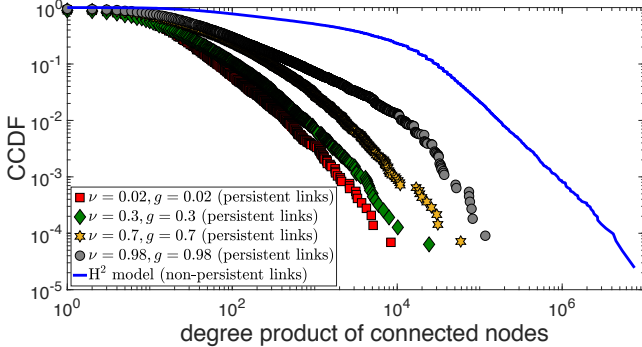


FIG. 6. Complementary cumulative distribution function (CCDF) of the degree product $k_1 \times k_2$ of nodes connected by persistent and non-persistent links. The results correspond to the persistent links in layer 2 of the multiplexes of Fig. 5, and to the links (non-persistent) in a network constructed with the \mathbb{H}^2 model with the same parameters as layer 2.

C. Average degree in layer 2

The resulting average degree in layer 2, $\tilde{\tilde{k}}_2$, is:

$$\tilde{\tilde{k}}_2 = N \int_0^{2R_2} p_2^{\text{all}}(x_2) f_2(x_2) dx_2 = \bar{k}_2 + w(\bar{k}_1 - \bar{k}_o), \quad (28)$$

where \bar{k}_2 from Eq. (5) and:

$$\bar{k}_o = N \int_0^{2R_2} \int_0^{2R_1} p_1(x_1) p_2(x_2) f(x_1|x_2) f_2(x_2) dx_1 dx_2$$

is the average local edge overlap between the two layers due to distance correlations. If there are no distance correlations, $\bar{k}_o = (\bar{k}_1 \bar{k}_2)/N \rightarrow 0$ as $N \rightarrow \infty$ and $\bar{k}_2 = \bar{k}_2 + w\bar{k}_1$. On the other hand, if the topologies of the two layers are identical, $\bar{k}_o = \bar{k}_1 = \bar{k}_2$ and $\tilde{\tilde{k}}_2 = \bar{k}_2$. Therefore, $\bar{k}_2 < \tilde{\tilde{k}}_2 < \bar{k}_2 + w\bar{k}_1$, and we can tune $\tilde{\tilde{k}}_2$ by tuning \bar{k}_2 . We note that for $w > 0$ we need a lower \bar{k}_2 to achieve the same $\tilde{\tilde{k}}_2$ as for $w = 0$ where $\tilde{\tilde{k}}_2 = \bar{k}_2$. A lower \bar{k}_2 corresponds to a higher hyperbolic disc radius R_2 (Eq. (5)), which explains the small differences in the R_2 s of the original and embedded synthetic multiplexes in Fig. 2—in the embeddings $w = 0$ as we do not account for link persistence.

D. Trans-layer connection probabilities

Let's turn our attention now to the trans-layer connection probabilities. The trans-layer connection probability among connected layer 1 pairs, $p_{\text{trans}}^c(x_1)$, can be written as:

$$p_{\text{trans}}^c(x_1) = w + (1 - w) \int_0^{2R_2} f(x_2|x_1) p_2(x_2) dx_2, \quad (29)$$

where $f(x_2|x_1)$ is the PDF of the hyperbolic distance x_2 of a pair in layer 2 conditioned on its distance x_1 in layer 1, and $p_2(x_2)$ in Eq. (13). If there are distance correlations, the second term in Eq. (29) decreases with x_1 since $f(x_2|x_1)$ concentrates over higher x_2 values and $p_2(x_2)$ decreases with x_2 . The stronger the correlations the faster the decrease. In the uncorrelated case, $f(x_2|x_1) = f_2(x_2)$, and:

$$p_{\text{trans}}^c(x_1) = w + (1 - w) \frac{\bar{k}_2}{N} \approx w, \quad (30)$$

in sparse networks ($\bar{k}_2 \ll N$). In the maximally correlated case, $f(x_2|x_1) = \delta(x_2 - x_1)$, and:

$$\begin{aligned} p_{\text{trans}}^c(x_1) &= w + (1 - w) p_2(x_1) \\ &= p_2(x_1) + (1 - p_2(x_1))w. \end{aligned} \quad (31)$$

In the above relation, $p_{\text{trans}}^c(x_1) \approx (1 - p_2(x_1))w \approx w$ for $x_1 \gg R_2 - 2T_2 \ln w$, while for $x_1 \ll R_2 - 2T_2 \ln w$, $p_{\text{trans}}^c(x_1) \approx p_2(x_1)$.

Taken altogether, from the above analysis we can conclude that: (i) no matter the correlation strengths, at large distances $x_1 \gg R_2$, $p_{\text{trans}}^c(x_1) \approx w$; and (ii) at smaller x_1 , $p_{\text{trans}}^c(x_1) \geq w$ and has an increasing trend if there are distance correlations (due to the second term in Eq. (29))—the stronger the correlations the higher the increase. These conclusions are validated in Fig. 7 and are consistent with our empirical observations in Fig. 1.

⁴ In sparse networks $\bar{k}_1 \propto \bar{k}_{0,2} \propto \bar{k}_2 \ll N$ while $R_2 \propto \ln N$.

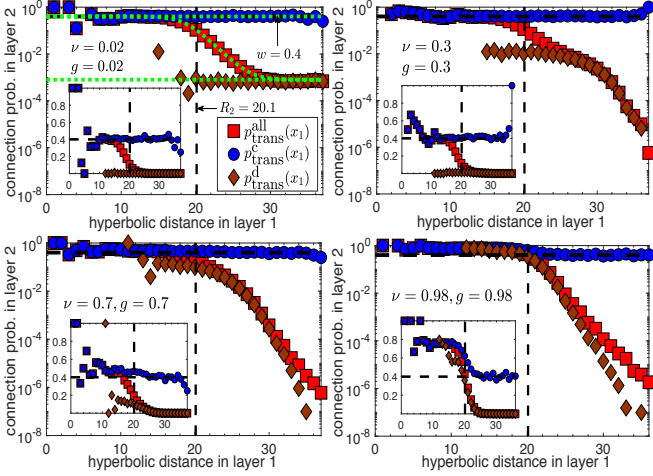


FIG. 7. Trans-layer connection probabilities $p_{\text{trans}}^{\text{all}}(x_1)$, $p_{\text{trans}}^{\text{c}}(x_1)$, $p_{\text{trans}}^{\text{d}}(x_1)$ at different correlation strengths. The results correspond to the synthetic multiplexes of Fig. 5. The y -axes in the plots are in log-scale, while the insets show the same results in linear scale. The green dotted lines in the first plot ($\nu = g = 0.02$) are the theoretical predictions for the uncorrelated case (Eqs. (30), (33) (35)).

The trans-layer connection probability among disconnected layer 1 pairs, $p_{\text{trans}}^{\text{d}}(x_1)$, is:

$$p_{\text{trans}}^{\text{d}}(x_1) = \int_0^{2R_2} f(x_2|x_1)p_2(x_2)dx_2. \quad (32)$$

As with the second term in Eq. (29), $p_{\text{trans}}^{\text{d}}(x_1)$ decreases with x_1 if there are distance correlations—the stronger the correlations the faster the decrease. In the uncorrelated case:

$$p_{\text{trans}}^{\text{d}}(x_1) = \frac{\bar{k}_2}{N}, \quad (33)$$

while in the maximally correlated case:

$$p_{\text{trans}}^{\text{d}}(x_1) = p_2(x_1). \quad (34)$$

This behavior is also validated in Fig. 7 and it is consistent with our empirical observations in Fig. 1. Finally, the trans-layer connection probability across all layer 1 pairs can be written as:

$$p_{\text{trans}}^{\text{all}}(x_1) = p_1(x_1)p_{\text{trans}}^{\text{c}}(x_1) + (1 - p_1(x_1))p_{\text{trans}}^{\text{d}}(x_1). \quad (35)$$

E. Estimating the link persistence probability w in real multiplexes

Our analysis shows that at large distances $x_1, x_2 \gg R_2$, $p_{\text{trans}}^{\text{c}}(x_1) \approx w$, $p_2^{\text{c}}(x_2) \approx w$. For each of the layer pairs in Fig. 1 we have estimated w as the average of the empirical $p_{\text{trans}}^{\text{c}}(x_1)$ at distances $x_1 > R_2$. The estimates of w are shown by the horizontal dashed lines in Fig. 1 and are

also reported in Table II (w_{12}). We have chosen $p_{\text{trans}}^{\text{c}}(x_1)$ for the estimation instead of $p_2^{\text{c}}(x_2)$ since as explained in Sec. IV, the former appears less prone to independent layer embedding effects. Table II also shows the standard deviation of $p_{\text{trans}}^{\text{c}}(x_1)$ at $x_1 > R_2$ ($\sigma_{w_{12}}$), as well as the estimated link persistence probability (w_{21}) and standard deviation ($\sigma_{w_{21}}$) in the direction from layer 2 to 1.

Multiplex	w_{12}	$\sigma_{w_{12}}$	w_{21}	$\sigma_{w_{21}}$
Internet	0.38	0.08	0.71	0.11
arXiv	0.71	0.06	0.82	0.10
Physicians	0.475	0.16	0.58	0.17
Drosophila	0.27	0.12	0.31	0.11
C. Elegans	0.20	0.13	0.09	0.06
Human Brain	0.35	0.18	0.42	0.13

TABLE II. Estimated link persistence probability w_{ij} from layer i to j , $i, j = 1, 2$, in the considered multiplexes. The estimated w_{ij} is the average of the empirical $p_{\text{trans}}^{\text{c}}(x_i)$ at distances $x_i > R_j$, while $\sigma_{w_{ij}}$ is the standard deviation of $p_{\text{trans}}^{\text{c}}(x_i)$ at $x_i > R_j$. The empirical $p_{\text{trans}}^{\text{c}}(x_i)$, $i = 1, 2$, is computed as in Fig. 1.

VII. IMPROVING TRANS-LAYER LINK PREDICTION

The results of Sec. VID suggest that we can improve *trans-layer link prediction*, i.e., the prediction of whether two nodes are connected in one layer of a multiplex, if we know the hyperbolic distance between the same nodes in another independently embedded layer, and whether the two nodes are connected in that layer. Specifically, from Eqs. (29), (32) we see that for each pair of nodes i, j in layer 1 we can assign a score:

$$s_{ij} = \psi(x_1^{ij}) + [1 - \psi(x_1^{ij})]w\alpha_{ij,1}, \quad (36)$$

where $\alpha_{ij,1}$ is the adjacency matrix of layer 1, while $0 \leq \psi(x_1^{ij}) \leq 1$ is a decreasing function of the hyperbolic distance between i, j in layer 1, x_1^{ij} . The higher the s_{ij} the higher is the likelihood that i and j are connected in layer 2.

Eq. (36) combines two mechanisms for link prediction. The first uses the fact that hyperbolicly closer nodes in layer 1 have higher chances of being connected in layer 2. Eqs. (29), (32) suggest that $\psi(x_1)$ is given by Eq. (32), which requires knowledge of the conditional density $f(x_2|x_1)$ and the connection probability $p_2(x_2)$. However, since in link prediction it is only the relative score among pairs that matters, we can use any monotonously decreasing function $\psi(x_1)$ in Eq. (36), which does not require the aforementioned knowledge. The second mechanism takes link persistence into account. In isolation, it predicts the existence of a link between two nodes in layer 2 with probability w if the

nodes are connected in layer 1, and with probability 0 otherwise.

The balance between the two mechanisms depends on the value of w and the choice of $\psi(x_1)$. Below, we consider the function:

$$\psi(x_1) = e^{-x_1}. \quad (37)$$

From Eqs. (36), (37) the score for the set of connected layer 1 pairs is given by $w + (1 - w)e^{-x_1}$, while for the disconnected pairs by e^{-x_1} . For each set of pairs the score decreases with the hyperbolic distance x_1 . At $x_1 \geq \ln(1/w)$ the score among disconnected pairs is always smaller than the score among connected pairs. At smaller x_1 , disconnected pairs can have a higher score than connected pairs at larger x_1 . Therefore, w in Eq. (36) can be seen as a “mixing” parameter that mixes the ordering of the scores of the two sets of pairs. At $w = 0$ link persistence is ignored, while at $w = 1$ all connected pairs are assigned the maximum score 1. The case where distance correlations are ignored is equivalent to choosing $\psi(x_1) = C$, where C is a constant, $0 \leq C < 1$.

In Fig. 8 we quantify the quality of trans-layer link prediction in the real multiplexes of Fig. 1. To this end, we use the *Area Under the Receiver Operating Characteristic Curve* (AUROC) and the *Area Under the Precision-Recall Curve* (AUPR) [44], computed over the set of common nodes in the two layers. The AUROC represents the probability that a randomly selected link from the set of links among the common nodes in layer 2 is given a higher score than a randomly selected nonexistent link, where the “non-existent” links are the disconnected common node pairs in layer 2. The degree to which the AUROC exceeds 0.5 indicates how much better the method performs than pure chance, while $\text{AUROC} = 1$ is the best possible AUROC. The AUPR represents how accurately one can classify layer 2 pairs as connected and disconnected based on their scores. It is a standard metric used when classes are imbalanced, i.e., when the number of negatives (disconnected pairs) is significantly larger than the number of positives (connected pairs), as in our case. The higher the AUPR the better the model is, while a perfect classifier has $\text{AUPR} = 1$. See [44] for further details.

Fig. 8 shows the AUROC and AUPR as a function of w if we use the scores prescribed by Eqs. (36), (37) (hyperbolic). The same figure also shows the results if instead of Eq. (37) we use $\psi(x_1) = 0$, which results in a simple binary link predictor, where if a link exists between two common nodes in layer 1, we predict that this link will also exist in layer 2 (binary). We see in Fig. 8 that by taking both hyperbolic distance correlations and link persistence into account we can improve trans-layer link prediction, especially with respect to AUPR. Specifically, we see that for $w > 0$ the hyperbolic AUPR improves and it is higher than the binary AUPR in all cases; in *Drosophila* and *C. Elegans* it is higher even at $w = 0$. The hyperbolic AUROC is significantly higher than the binary AUROC in all cases (even at $w = 0$), except from

the Human Brain, and it improves at $w > 0$.

We also see that in all cases the performance of prediction is virtually the same for the considered values of $w \in (0, 1)$. This is expected since as explained, for $x_1 \geq \ln(1/w)$ connected layer 1 pairs are always ranked higher (have a better score) than disconnected pairs. As the majority of disconnected pairs are separated by large x_1 distances, this condition is expected to hold even for small values of $w > 0$ (e.g., $w = 0.01$). Furthermore, w does not affect the relative ranking within each set of pairs. In other words, the considered values of $w \in (0, 1)$ are not expected to significantly affect the overall ranking across node pairs, which justifies the observed behavior. As also explained, when $w = 1$ we ignore the distances among connected layer 1 pairs, which are all assigned the same score 1. We see that in this case the AUPR decreases in all cases, except from the Physicians. In general, one would require learning the optimal value(s) of w for a specific option of $\psi(x_1)$ in Eq. (37) using a training set of layer 2 links. Exploring other options for $\psi(x_1)$ is beyond the scope of this paper.

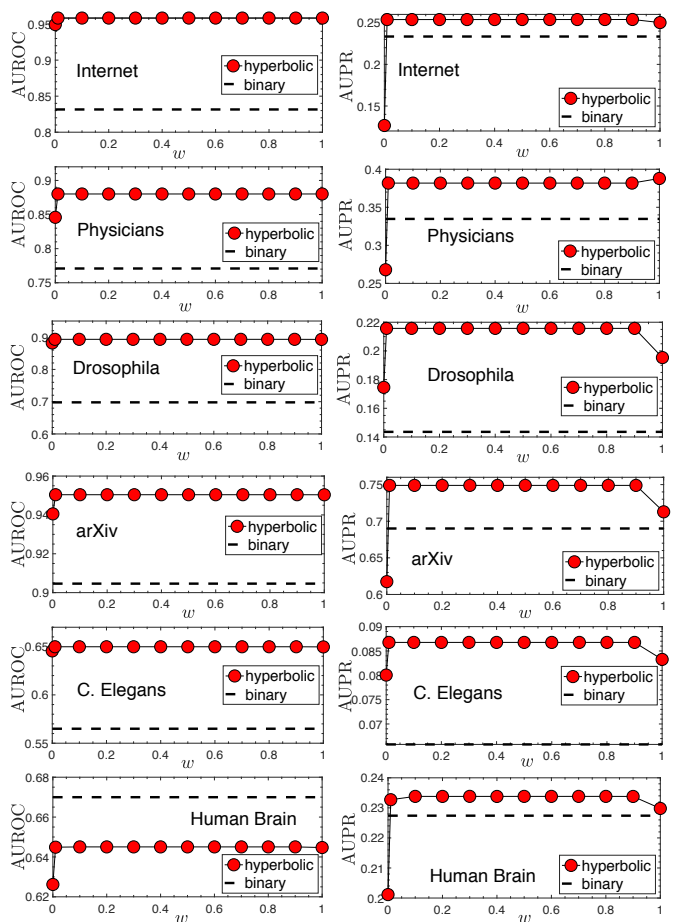


FIG. 8. Trans-layer link prediction (layer 1 to layer 2) in the multiplexes of Fig. 1. **Left column:** Area Under the Receiver Operating Characteristic Curve (AUROC). **Right column:** Area Under the Precision-Recall Curve (AUPR).

VIII. DISCUSSION AND CONCLUSION

We have seen that GMM-LP can reproduce the link-persistence behavior observed in real multiplexes remarkably well. In addition to geometric correlations, in GMM-LP the explicit link formation process in layer 1 impacts the formation of links in layer 2. As a result, the connection probability in layer 2 differs from the one in the \mathbb{H}^2 model (Eq. (22) vs. Eq. (13)). Specifically, in GMM-LP one can view link persistence as “noise” imposed to the tail of the connection probability of the \mathbb{H}^2 model, allowing connections at larger distances with higher probability. The stronger the distance correlations among the layers the weaker the effect of link persistence is, i.e., the lower the probability for longer distance connections (Figs. 5(a),(b)). In this sense, link persistence has a similar effect as temperature in the \mathbb{H}^2 model, and does not significantly affect the main topological properties of layer 2, which are similar to those in the \mathbb{H}^2 model (Figs. 5(c),(d)). An outstanding question is whether there exists a model that can capture the link-persistence behavior of real systems while preserving the connection probability of the \mathbb{H}^2 model in the layers.

We have also seen that link persistence can explain the high edge overlap in real systems, which cannot be explained by coordinate correlations alone (Fig. 4). Specifically, to achieve the same overlap in synthetic systems without link persistence, we need significantly higher correlation strengths than those in Table I. Furthermore, in some cases we cannot achieve the same overlap even with maximal correlations. We note that this result does not contradict the work in [45], which shows that high edge overlap naturally emerges among layers embedded in Euclidean spaces, where nodes have the same coordinates in each layer. In fact, our results also suggest that high overlap without link persistence can emerge in cases where the node coordinates are very strongly correlated across layers and the layers have sufficiently low temperatures. However, this is not the case with the considered real systems (Fig. 4). In addition, we have seen that by taking both link persistence and hyperbolic distance correlations into account we can improve trans-layer link prediction (Fig. 8).

All considered models (\mathbb{H}^2 , GMM, GMM-LP) use for simplicity a uniform distribution for the angular similarity coordinates. This leads to generated topologies without community structure [7, 46, 47]. On the other hand, the considered real layers (Table I) exhibit community structure and trans-layer community correlations, which are manifested in their embeddings as groups of nodes that are similar—close along the angular similarity direction—in both layers simultaneously [14, 48]. It would be interesting to modify the assignment of angular coordinates in the GMM-LP along the lines of [46] so that the model can also generate synthetic layers with community correlations. Community correlations are expected to promote the overlap among intra-community links, without however explaining the observed link per-

sistence that occurs irrespectively of the hyperbolic distances that the connections span (cf. Fig. 1).

The work in [49] considers link persistence (also called stability) in dynamic networks, in conjunction with node hidden variables (or fitnesses) that determine the nodes’ capability of forming links. For each network snapshot in [49] both connections and disconnections can be copied from the previous snapshot with a certain probability, or formed with a probability that depends on the nodes’ fitnesses. Similarly to our work, this work also attempts to disentangle the importance of the two mechanisms (link persistence vs. node hidden variables) in link formation. However, differently from our work, it does not consider multiplex networks, nor networks embedded into hyperbolic spaces, i.e., networks where the node hidden variables are their coordinates in their underlying hyperbolic space. Furthermore, it does not analyze the effect of link persistence to the resulting topological properties of the network. Finally, in [49] both connections (links) and disconnections (non-links) can persist (copied) from one snapshot to another with possibly different probabilities. In GMM-LP only connections can persist from one layer to another, with the same probability w . It appears that this simple mechanism is sufficient for reproducing the link-persistence behavior observed in real systems. In future work, it would be interesting to investigate the reasons behind the variability of w across different real systems and layers (cf. Table II).

Our results guide the development of multiplex embedding methods, in which the layers of a multiplex are simultaneously and not independently embedded into hyperbolic spaces, suggesting that such methods should be accounting for both coordinate correlations and link persistence across layers. An important aspect of multiplex embeddings is that they can improve link prediction in the individual layers compared to the case where the layers are embedded independently, cf. [50]. Further, they could potentially lead to improved multidimensional community detection on a geometric basis and yield more realistic multilayer greedy routing success rates [14], as they are expected to better capture the relation between the layers. To infer the hyperbolic node coordinates $\{r_{2,i}, \theta_{2,i}\}$ for each node $i = 1, \dots, N$ in layer 2 of GMM-LP, along with the correlation strengths ν, g and the link persistence probability w , one needs to maximize a conditional likelihood of the form:

$$\begin{aligned} \mathcal{L}_{\text{cond}} \propto & \text{Prob}(\{r_{2,i}, \theta_{2,i}\} | \{r_{1,i}, \theta_{1,i}\}, \nu, g) \\ & \times \mathcal{L}(\alpha_{ij,2} | \{r_{i,2}, \theta_{i,2}\}, \alpha_{ij,1}, w). \end{aligned} \quad (38)$$

The first term in the above relation is the PDF of the node coordinates in layer 2 conditioned on their values in layer 1 and the correlation strengths:

$$\begin{aligned} \text{Prob}(\{r_{2,i}, \theta_{2,i}\} | \{r_{1,i}, \theta_{1,i}\}, \nu, g) = & \prod_{1 \leq i \leq N} \rho_2(r_{2,i} | r_{1,i}, \nu) \\ & \times \prod_{1 \leq i \leq N} f(\theta_{2,i} | \theta_{1,i}, g), \end{aligned}$$

where $\rho_2(r_{2,i}|r_{1,i}, \nu)$ in Eq. (8) and:

$$f(\theta_{2,i}|\theta_{1,i}, g) = \frac{N}{2\pi} f_g \left(\frac{N}{2\pi} (\pi - |\pi - |\theta_{2,i} - \theta_{1,i}||) \right),$$

where $f_g(l)$ in Eq. (11). The second term in Eq. (38), $\mathcal{L}(\alpha_{ij,2}|\{r_{i,2}, \theta_{i,2}\}, \alpha_{ij,1}, w) \equiv \mathcal{L}_2$, is the likelihood to have the network adjacency matrix $\alpha_{ij,2}$ in layer 2 if the node coordinates have the values $\{r_{i,2}, \theta_{i,2}\}$, the adjacency matrix of layer 1 is $\alpha_{ij,1}$, and the link persistence probability is w :

$$\begin{aligned} \mathcal{L}_2 = & \prod_{1 \leq j < i \leq N} [w\alpha_{ij,1}\alpha_{ij,2} + (1 - w\alpha_{ij,1})p_2(x_2^{ij})^{\alpha_{ij,2}} \\ & \times (1 - p_2(x_2^{ij}))^{1-\alpha_{ij,2}}]. \end{aligned} \quad (39)$$

The above product goes over all node pairs in layer 2, while $p_2(x_2^{ij})$ is given in Eq. (13). An initial estimate of w can be obtained using the procedure in Sec. VI E. We leave this maximization problem open for future work.

ACKNOWLEDGMENTS

F. P. acknowledges support by the EU H2020 NOTRE project (grant 692058). K.-K. K. acknowledges support by the EU H2020 Program under the funding scheme FET-PROACT-1-2014: Global Systems Science (GSS), grant agreement 641191 CIMPLEX: Bringing Citizens, Models and Data together in Participatory, Interactive Social EXploratories.

Appendix A: Real-world multiplex network data

Here we provide details on the considered real-world multiplex network data. For further details see [14].

IPv4/IPv6 Internet. The IPv4 and IPv6 Autonomous Systems (AS) Internet topologies were extracted from the data collected by CAIDA [28, 51]. The connections in each topology are not physical but logical, representing AS relationships. The IPv4 dataset consists of ASs that can route Internet packets with IPv4 destination addresses, while the IPv6 dataset consists of ASs that can route packets with IPv6 destination addresses. The considered topologies correspond to January 2015. The IPv4 topology (layer 1) consists of $N_1 = 37563$ nodes (ASs), and has a power law degree distribution with exponent $\gamma_1 = 2.1$, average node degree $\bar{k}_1 = 5.06$, and average clustering $\bar{c}_1 = 0.63$ ($T_1 = 0.5$).⁵ The IPv6 topology (layer 2) consists of $N_2 = 5162$ nodes, has a power law degree distribution with exponent $\gamma_2 = 2.1$, average node degree $\bar{k}_2 = 5.21$, and average clustering $\bar{c}_2 = 0.55$ ($T_2 = 0.5$). There are 4819 common nodes in the two

topologies, i.e., ASs that can route both IPv4 and IPv6 packets.

Drosophila Melanogaster. The *Drosophila Melanogaster* dataset is taken from [30, 52]. In this dataset, the networks represent protein-protein interactions and the layers correspond to interactions of different nature. Layer 1 corresponds to suppressive genetic interaction, while layer 2 corresponds to additive genetic interaction. Layer 1 has $N_1 = 839$ nodes, average degree $\bar{k}_1 = 4.43$, and average clustering $\bar{c}_1 = 0.28$ ($T_1 = 0.68$). Its degree distribution can be approximated by a power law with exponent $\gamma_1 = 2.6$. Layer 2 has $N_2 = 755$ nodes, average degree $\bar{k}_2 = 3.77$, and average clustering $\bar{c}_2 = 0.29$ ($T_2 = 0.65$). Its degree distribution can be approximated by a power law with exponent $\gamma_2 = 2.8$. There are 557 common nodes in the two layers.

C. Elegans Connectome. The *C. Elegans* dataset is taken from [53, 54]. It corresponds to the neuronal network of the nematode *Caenorhabditis Elegans*. The nodes are neurons and each layer corresponds to a different type of synaptic connection: Electric (layer 1) and Chemical Monadic (layer 2). Layer 1 has $N_1 = 253$ nodes, average degree $\bar{k}_1 = 4.06$, and average clustering $\bar{c}_1 = 0.24$ ($T_1 = 0.65$). Layer 2 has $N_2 = 260$ nodes, average degree $\bar{k}_2 = 6.83$, and average clustering $\bar{c}_2 = 0.21$ ($T_2 = 0.7$). The degree distribution in both layers can be approximated by a power law with exponent $\gamma_1 = \gamma_2 = 2.9$. There are 238 common nodes in the two layers.

Human Brain. The human brain data is taken from [55]. The data consists of a structural (anatomical) network, as well as a functional network. In both networks, nodes are brain regions. The structural network (layer 1) consists of 85 nodes, with average degree $\bar{k}_1 = 5.41$, maximum degree $k_1^{\max} = 12$, and average clustering $\bar{c}_1 = 0.49$ ($T_1 = 0.4$). The functional network (layer 2) has 80 nodes, average degree $\bar{k}_2 = 5.48$, maximum degree $k_2^{\max} = 14$, and average clustering $\bar{c}_2 = 0.40$ ($T_2 = 0.5$). The two layers have 77 nodes in common and $\gamma_1 = \gamma_2 = 6$.

arXiv. The arXiv data is taken from [56] and contains co-authorship networks. The nodes are authors that are connected if they have co-authored a paper. In arXiv, each paper is assigned to one or more relevant categories. The data considers only papers with the word “networks” in the title or abstract from different categories up to May 2014. In the considered data, layer 1 corresponds to the network formed by the authors of papers in the ‘Disordered Systems and Neural Networks’ (cond-mat.dis-nn) category and layer 2 corresponds to “Biological Physics” (physics.bio-ph). The corresponding size, average degree, average clustering, and power law exponent for each layer are $N_1 = 3506$, $N_2 = 2956$, $\bar{k}_1 = 4.19$, $\bar{k}_2 = 4.13$, $\bar{c}_1 = 0.81$, $\bar{c}_2 = 0.83$ ($T_1 = T_2 = 0.05$), and $\gamma_1 = \gamma_2 = 2.6$. There are 1514 common nodes in the two layers.

Physicians. The Physicians dataset is taken from [57]. The network layers correspond to different types of relations among physicians in four US towns.

⁵ The average clustering is calculated excluding nodes of degree 1.

In the considered data, layers 1, 2 correspond respectively to discussion and advice relations among the physicians. The corresponding size, average degree, average clustering, and power law exponent for each layer are $N_1 = 231, N_2 = 215, \bar{k}_1 = 4.31, \bar{k}_2 = 4.18, \bar{c}_1 = \bar{c}_2 = 0.28$ ($T_1 = T_2 = 0.65$), and $\gamma_1 = 2.8, \gamma_2 = 2.7$. There are 212 common nodes in the two layers.

In all hyperbolic embeddings of both real and synthetic layers, the angular node coordinates are obtained using HyperMap [18, 41]. The radial coordinate r_i of each node i is obtained from Eq. (4) after setting $\bar{k}(r_i) = \kappa_i \equiv \max\{\bar{k}_0, k_i - \gamma T\}$, where k_i is the observed degree of the node in the layer [10]. In other words, we use the inferred radial coordinates prescribed by the static \mathbb{H}^2 model [10] that we work with, instead of the ones obtained by HyperMap that are akin to the growing popularity \times similarity model [3].

Appendix B: Conditional PDF of radial coordinates

Here we derive Eq. (8). We note that the GMM [14] uses the \mathbb{S}^1 model [58], where instead of a radial coordinate r_i each node i has a hidden degree variable κ_i . The degree variables are then transformed to radial coordinates in the \mathbb{H}^2 model, which is isomorphic to the \mathbb{S}^1 , via Eq. (4) after setting $\bar{k}(r_i) = \kappa_i$. Here we work directly with radial coordinates.

By integrating the PDFs of the radial coordinates in layers 1 and 2, $\rho_1(r_1), \rho_2(r_2)$ (Eqs. (6), (9)), we get the corresponding CDFs:

$$F_1(r_1) \approx e^{-\phi_1}, \phi_1 \equiv \frac{R_1 - r_1}{2\beta_1}, \quad (\text{B1})$$

$$F_2(r_2) \approx e^{-\phi_2}, \phi_2 \equiv \frac{R_2 - r_2}{2\beta_2}. \quad (\text{B2})$$

To derive the joint PDF of the radial coordinates we use the bivariate Gumbel-Hougaard copula as in [14], defined as:

$$C_\eta(r_1, r_2) = e^{-[(-\ln F_1(r_1))^\eta + (-\ln F_2(r_2))^\eta]^{\frac{1}{\eta}}} \\ = e^{-(\phi_1^\eta + \phi_2^\eta)^{\frac{1}{\eta}}}, \eta \equiv \frac{1}{1 - \nu} \in [1, \infty), \quad (\text{B3})$$

where $\nu \in [0, 1)$ is the radial correlation strength parameter. The joint PDF of r_1 and r_2 , $\rho_\eta(r_1, r_2)$, can be obtained by differentiating $C_\eta(r_1, r_2)$ with respect to r_1 and r_2 . The conditional PDF in Eq. (8) is obtained as $\rho_2(r_2|r_1, \eta) = \rho_\eta(r_1, r_2)/\rho_1(r_1)$.

Appendix C: $\tilde{k}_2(r)$ in the uncorrelated and maximally correlated cases

The last approximation for the hyperbolic distance in Eq. (3) allows us to write the connection probability in

layer $i = 1, 2$ as:

$$p_i(r, r', \Delta\theta) \approx \frac{1}{1 + \left(\frac{\Delta\theta}{2} e^{\frac{1}{2}(r+r'-R_i)}\right)^{1/T_i}}. \quad (\text{C1})$$

Using the fact that $\int_0^\infty 1/(1 + \chi^{\frac{1}{T}})d\chi = T\pi/\sin T\pi$ for $T < 1$, and that the angular distance $\Delta\theta$ is uniformly distributed on $[0, \pi]$, we can write:

$$\frac{1}{\pi} \int_0^\pi p_i(r, r', \Delta\theta)d\Delta\theta \approx \frac{2T_i}{\sin T_i\pi} e^{-\frac{1}{2}(r+r'-R_i)}. \quad (\text{C2})$$

Using Eqs. (C2) and (9) yields:

$$\frac{N}{\pi} \int_0^{R_2} \rho_2(r')dr' \int_0^\pi p_2(r, r', \Delta\theta)d\Delta\theta \approx \bar{k}_2(r), \quad (\text{C3})$$

$$\frac{N}{\pi} \int_0^{R_2} \rho_2(r')dr' \int_0^\pi p_1(r, r', \Delta\theta)d\Delta\theta \approx C\bar{k}_2(r), \quad (\text{C4})$$

where $\bar{k}_2(r)$ in Eq. (25), $C = c_2 T_1 \sin T_2 \pi / (c_1 T_2 \sin T_1 \pi)$ and $c_i, i = 1, 2$ in Eq. (5). If the radial coordinates are identical in the two layers, $R_1 = R_2$, and $c_1 = c_2$.

Eq. (24) follows from Eqs. (20), (22), (23) and (C3). To derive Eq. (26) we also use the additional fact that $\int_0^\infty [1/(1 + \chi^{\frac{1}{T}})]^2 d\chi = (1 - T)T\pi/\sin T\pi$ for $T < 1$, which allows us to write:

$$\frac{N}{\pi} \int_0^{R_2} \rho_2(r')dr' \int_0^\pi p_2(r, r', \Delta\theta)^2 d\Delta\theta \\ \approx (1 - T_2)\bar{k}_2(r), \quad (\text{C5})$$

$$\frac{N}{\pi} \int_0^{R_2} \rho_2(r')dr' \int_0^\pi p_1(r, r', \Delta\theta)^2 d\Delta\theta \\ \approx (1 - T_1)C\bar{k}_2(r). \quad (\text{C6})$$

Using the above two relations and the Cauchy-Schwarz inequality we have:

$$\frac{N}{\pi} \int_0^{R_2} \rho_2(r')dr' \int_0^\pi p_1(r, r', \Delta\theta)p_2(r, r', \Delta\theta)d\Delta\theta \\ \leq \bar{k}_2(r)\sqrt{C(1 - T_1)(1 - T_2)}. \quad (\text{C7})$$

Eq. (26) follows from Eqs. (21), (22), (23), (C3), (C4) and (C7). If in addition $T_1 = T_2$, $p_1(r, r', \Delta\theta) = p_2(r, r', \Delta\theta)$, $C = 1$, and Eq. (27) follows from Eqs. (21), (22), (23), (C3), (C4) and (C5).

Appendix D: Conditional hyperbolic distance PDF

Finally, in this section we show how to compute $f(x_2|r_1, r'_1, \Delta\theta_1)$, which is the PDF of the hyperbolic distance x_2 between two nodes in layer 2 conditioned on the nodes' radial coordinates r_1, r'_1 and angular distance $\Delta\theta_1$ in layer 1. This conditional PDF does not have an analytic expression and we show here how to compute it using numerical integration. To this end, we first need

to derive $P(\Delta\theta_2 \leq \Delta\theta|\Delta\theta_1)$, which is the CDF of the angular distance $\Delta\theta_2$ of a pair in layer 2 conditioned on its angular distance $\Delta\theta_1$ in layer 1. This CDF admits an analytic expression. As we explain (Appendix D3), the conditional PDF $f(x_2|x_1)$, where x_1 is the hyperbolic distance between the pair in layer 1, can be obtained by integrating $f(x_2|r_1, r'_1, \Delta\theta_1)$ over r_1, r'_1 .

1. Conditional CDF $P(\Delta\theta_2 \leq \Delta\theta|\Delta\theta_1)$

Let $\Delta\theta_1$ and $\Delta\theta_2$ be random variables denoting respectively the angular distance between the same pair of nodes in layers 1 and 2, whose angles are θ_1, θ'_1 (layer 1) and θ_2, θ'_2 (layer 2). From Eq. (10) and the fact that $\Delta\theta_2 = \pi - |\pi - |\theta_2 - \theta'_2||$, we can see that $\Delta\theta_2$ is obtained by first moving the points at θ_1 and θ'_1 on the circle by $2\pi l/N$ and $2\pi l'/N$, respectively, and then computing the angular distance between the new points. Equivalently, we can view $\Delta\theta_2$ as being obtained by first computing the angular distance between the points at θ_1 and θ'_1 , $\Delta\theta_1 = \pi - |\pi - |\theta_1 - \theta'_1||$, and then adding to this distance the term $2\pi\tilde{l}/N$, where $\tilde{l} = l - l'$. The PDF of \tilde{l} can be obtained from the PDFs of l, l' (Eq. (11)):

$$\begin{aligned} \tilde{f}_g(\tilde{l}) &= \frac{d}{d\tilde{l}} \left(\int_{-\frac{N}{2}}^{\frac{N}{2}} \int_{-\frac{N}{2}}^{\tilde{l}+l'} f_g(l) f_g(l') dl dl' \right) \\ &= \frac{\phi\left(\frac{\tilde{l}}{\sqrt{2}\sigma}\right)}{2\sqrt{2}\sigma} \left[\frac{\operatorname{erf}\left(\frac{N-\tilde{l}}{2\sigma}\right) + \operatorname{erf}\left(\frac{N+\tilde{l}}{2\sigma}\right)}{\operatorname{erf}\left(\frac{N}{\sqrt{2}\sigma}\right)^2} \right] \\ &\approx \frac{\phi\left(\frac{\tilde{l}}{\sqrt{2}\sigma}\right)}{\sqrt{2}\sigma \operatorname{erf}\left(\frac{N}{4\sigma}\right)}. \end{aligned} \quad (\text{D1})$$

In other words, the PDF of $\tilde{l} \in [-N/2, N/2]$ is approximately the same as Eq. (11) except that its variance is $2\sigma^2$. Therefore, we can write:

$$\Delta\theta_2 \stackrel{d}{=} \pi - |\pi - \operatorname{mod} \left[\Delta\theta_1 + \frac{2\pi\tilde{l}}{N}, 2\pi \right]|, \quad (\text{D2})$$

where \tilde{l} is sampled from Eq. (D1) and the symbol $\stackrel{d}{=}$ means *equal in distribution*.

Eq. (D2) suggests that for a given $\Delta\theta_1$, $\Delta\theta_2$ is Gaussian with mean $\Delta\theta_1$ and variance $\tilde{\sigma}^2 = (2\pi/N)^2 2\sigma^2$. In fact, it is a *folded Gaussian* [59] since probability mass is “folded” at 0. Specifically, when $\Delta\theta_1 + 2\pi\tilde{l}/N \in [-\pi, 0)$, $\Delta\theta_2 = |\Delta\theta_1 + 2\pi\tilde{l}/N| \in (0, \pi]$. Further, probability mass is also folded at π , since when $\Delta\theta_1 + 2\pi\tilde{l}/N \in (\pi, 2\pi]$, $\Delta\theta_2 = 2\pi - \Delta\theta_1 - 2\pi\tilde{l}/N \in [0, \pi)$. Using the PDF of a folded Gaussian [59] we can write:

$$\begin{aligned} f(\Delta\theta_2|\Delta\theta_1) &= \frac{e^{-\frac{(\Delta\theta_2 - \Delta\theta_1)^2}{2\tilde{\sigma}^2}} + e^{-\frac{(\pi - |\pi - \Delta\theta_2 - \Delta\theta_1|)^2}{2\tilde{\sigma}^2}}}{K\sqrt{2\pi}\tilde{\sigma}}, \quad (\text{D3}) \\ \tilde{\sigma} &= \frac{2\sqrt{2}\pi\sigma}{N}, \quad K = \operatorname{erf}\left(\frac{N}{4\sigma}\right), \end{aligned}$$

where K is the normalizing constant such that $\int_0^\pi f(\Delta\theta_2|\Delta\theta_1) d\Delta\theta_2 = 1, \forall \Delta\theta_1 \in [0, \pi]$. The second term in the numerator of Eq. (D3) accounts for the folding at 0 when $-\pi \leq \Delta\theta_1 - \Delta\theta_2 < 0$ and at π when $\pi < \Delta\theta_1 + \Delta\theta_2 \leq 2\pi$. By integrating Eq. (D3) we get the CDF $P(\Delta\theta_2 \leq \Delta\theta|\Delta\theta_1)$:

$$\begin{aligned} P(\Delta\theta_2 \leq \Delta\theta|\Delta\theta_1) &= \frac{\operatorname{erf}\left(\frac{N(\Delta\theta - \Delta\theta_1)}{4\pi\sigma}\right) + \operatorname{erf}\left(\frac{N(\Delta\theta + \Delta\theta_1)}{4\pi\sigma}\right)}{2\operatorname{erf}\left(\frac{N}{4\sigma}\right)} \\ &\equiv P_1^g(\Delta\theta|\Delta\theta_1), \end{aligned} \quad (\text{D4})$$

if $\Delta\theta \leq \pi - \Delta\theta_1$, or, otherwise,

$$\begin{aligned} P(\Delta\theta_2 \leq \Delta\theta|\Delta\theta_1) &= 1 - \frac{\operatorname{erf}\left(\frac{N(2\pi - \Delta\theta - \Delta\theta_1)}{4\pi\sigma}\right)}{2\operatorname{erf}\left(\frac{N}{4\sigma}\right)} \\ &\quad + \frac{\operatorname{erf}\left(\frac{N(\Delta\theta - \Delta\theta_1)}{4\pi\sigma}\right)}{2\operatorname{erf}\left(\frac{N}{4\sigma}\right)} \equiv P_2^g(\Delta\theta|\Delta\theta_1). \end{aligned} \quad (\text{D5})$$

Eqs. (D4) and (D5) are validated in Fig. 9, perfectly matching simulations.

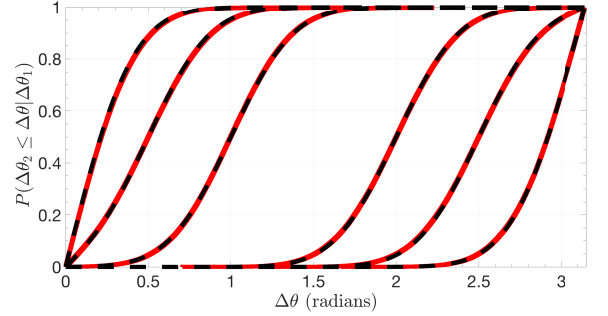


FIG. 9. Conditional angular distance CDF. The results are from a two layer synthetic multiplex with $N_1 = 5000$ and $N_2 = 3000$ nodes, and angular correlation strength $g = 0.5$. All nodes in the smaller layer also exist in the larger. The conditional CDFs from left to right correspond to $\Delta\theta_1 = 0.1, 0.5, 1.0, 2.0, 2.5, 3.0$ radians. The red solid lines are the empirical distributions while the dashed black lines are the corresponding theoretical predictions given by Eqs. (D4), (D5) with $N = N_2$.

2. Conditional PDF $f(x_2|r_1, r'_1, \Delta\theta_1)$

Now, consider two nodes with radial coordinates $r_1 \in [0, R_1]$, $r'_1 \in [0, R_1]$ and angular distance $\Delta\theta_1 \in [0, \pi]$ in layer 1. Further, let X_2 be a random variable denoting the hyperbolic distance x_2 between these nodes in layer 2, where their radial coordinates are $r_2 \in [0, R_2]$, $r'_2 \in [0, R_2]$, and their angular distance is $\Delta\theta_2 \in [0, \pi]$. Since $x_2 \approx r_2 + r'_2 + 2 \ln \sin(\Delta\theta_2/2)$ (Eq. (3)), we can

write the CDF of X_2 conditioned on $r_1, r'_1, \Delta\theta_1$ as:

$$P(X_2 \leq x_2 | r_1, r'_1, \Delta\theta_1) = \int \int P\left(\Delta\theta_2 \leq 2 \arcsin e^{\frac{1}{2}(x_2 - r_2 - r'_2)} | \Delta\theta_1\right) \times \rho_2(r'_2 | r'_1, \nu) \rho_2(r_2 | r_1, \nu) dr'_2 dr_2, \quad (\text{D6})$$

where $\rho_2(r_2 | r_1, \nu)$ in Eq. (8). The above integral can be evaluated numerically using Eqs. (D4) and (D5). To this end, we need to identify the different limits of integration and the corresponding integrands. To ease notation, let:

$$d\rho_\nu \equiv \rho_2(r'_2 | r'_1, \nu) \rho_2(r_2 | r_1, \nu) dr'_2 dr_2, \quad (\text{D7})$$

$$\widetilde{\Delta\theta}_2 \equiv 2 \arcsin e^{\frac{1}{2}(x_2 - r_2 - r'_2)}, \quad (\text{D8})$$

$$\tilde{x}_2 \equiv \min \left[x_2 - 2 \ln \sin \left(\frac{\pi - \Delta\theta_1}{2} \right), 2R_2 \right]. \quad (\text{D9})$$

We observe that $x_2 \leq \tilde{x}_2$. Furthermore, Eq. (D4) holds if $\tilde{x}_2 \leq r_2 + r'_2$, while Eq. (D5) holds if $r_2 + r'_2 \leq \tilde{x}_2$. Finally, $P(X_2 \leq x_2 | r_1, r'_1, \Delta\theta_1) = 1$ if $r_2 + r'_2 \leq x_2$.

Given the above observations we distinguish three cases: (i) $\tilde{x}_2 \leq R_2$; (ii) $x_2 \leq R_2 \leq \tilde{x}_2$; and (iii) $R_2 \leq x_2$. Using Eqs. (D4), (D5) and the notation in (D7)-(D9) we can write:

If $\tilde{x}_2 \leq R_2$:

$$P(X_2 \leq x_2 | r_1, r'_1, \Delta\theta_1) = \int_0^{\tilde{x}_2} \int_0^{R_2} P_1^g(\widetilde{\Delta\theta}_2 | \Delta\theta_1) d\rho_\nu + \int_0^{R_2} \int_0^{R_2} P_1^g(\widetilde{\Delta\theta}_2 | \Delta\theta_1) d\rho_\nu + \int_0^{x_2} \int_0^{\tilde{x}_2 - r_2} P_2^g(\widetilde{\Delta\theta}_2 | \Delta\theta_1) d\rho_\nu + \int_0^{\tilde{x}_2} \int_0^{\tilde{x}_2 - r_2} P_2^g(\widetilde{\Delta\theta}_2 | \Delta\theta_1) d\rho_\nu + \int_0^{x_2} \int_0^{x_2 - r_2} d\rho_\nu \equiv I_1(x_2 | r_1, r'_1, \Delta\theta_1);$$

if $x_2 \leq R_2 \leq \tilde{x}_2$:

$$P(X_2 \leq x_2 | r_1, r'_1, \Delta\theta_1) = \int_{\tilde{x}_2 - R_2}^{R_2} \int_{\tilde{x}_2 - r_2}^{R_2} P_1^g(\widetilde{\Delta\theta}_2 | \Delta\theta_1) d\rho_\nu + \int_0^{x_2} \int_{x_2 - r_2}^{R_2 - r_2} P_2^g(\widetilde{\Delta\theta}_2 | \Delta\theta_1) d\rho_\nu + \int_{x_2}^{R_2} \int_0^{R_2 - r_2} P_2^g(\widetilde{\Delta\theta}_2 | \Delta\theta_1) d\rho_\nu + \int_0^{\tilde{x}_2 - R_2} \int_{R_2 - r_2}^{\tilde{x}_2 - r_2} P_2^g(\widetilde{\Delta\theta}_2 | \Delta\theta_1) d\rho_\nu + \int_0^{x_2} \int_0^{x_2 - r_2} d\rho_\nu \equiv I_2(x_2 | r_1, r'_1, \Delta\theta_1);$$

and if $R_2 \leq x_2$:

$$P(X_2 \leq x_2 | r_1, r'_1, \Delta\theta_1) = \int_{\tilde{x}_2 - R_2}^{R_2} \int_{\tilde{x}_2 - r_2}^{R_2} P_1^g(\widetilde{\Delta\theta}_2 | \Delta\theta_1) d\rho_\nu + \int_{x_2 - R_2}^{\tilde{x}_2 - R_2} \int_{x_2 - r_2}^{R_2} P_2^g(\widetilde{\Delta\theta}_2 | \Delta\theta_1) d\rho_\nu + \int_{x_2 - R_2}^{\tilde{x}_2 - R_2} \int_{x_2 - r_2}^{R_2} P_2^g(\widetilde{\Delta\theta}_2 | \Delta\theta_1) d\rho_\nu + \int_0^{x_2 - R_2} \int_0^{x_2 - r_2} d\rho_\nu + \int_{x_2 - R_2}^{R_2} \int_0^{x_2 - r_2} d\rho_\nu \equiv I_3(x_2 | r_1, r'_1, \Delta\theta_1).$$

By differentiating the above relations with respect to x_2 we get the corresponding PDFs:

$$f_1(x_2 | r_1, r'_1, \Delta\theta_1) = \frac{dI_1(x_2 | r_1, r'_1, \Delta\theta_1)}{dx_2}, \quad (\text{D10})$$

$$f_2(x_2 | r_1, r'_1, \Delta\theta_1) = \frac{dI_2(x_2 | r_1, r'_1, \Delta\theta_1)}{dx_2}, \quad (\text{D11})$$

$$f_3(x_2 | r_1, r'_1, \Delta\theta_1) = \frac{dI_3(x_2 | r_1, r'_1, \Delta\theta_1)}{dx_2}. \quad (\text{D12})$$

The above analysis is validated in Fig. 10. To evaluate our integrals we use the Cuba library for multidimensional numerical integration [60, 61]. Our code computing both conditional CDFs and PDFs is available at [42].

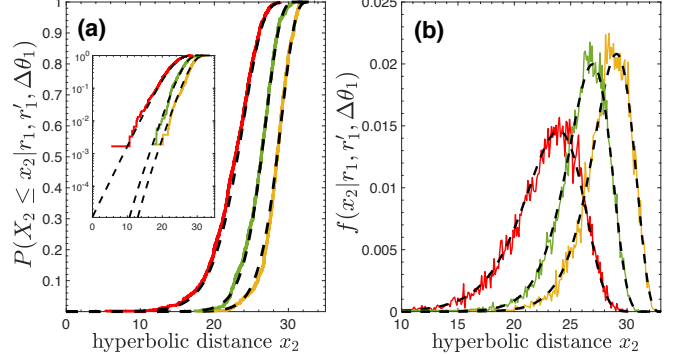


FIG. 10. The results are from a two layer synthetic multiplex with $N_1 = 5000$ and $N_2 = 3000$ nodes, $\gamma_1 = 2.1, \gamma_2 = 2.5, T_1 = T_2 = 0.5$ and $\bar{k}_1 = \bar{k}_2 = 6$ ($R_1 = 23, R_2 = 16.8$). The correlation strengths are $\nu = 0.5, g = 0.7$, and all nodes in the smaller layer also exist in the larger. The plots show conditional hyperbolic distance CDFs and PDFs (histograms) for $r_1 = 18, r'_1 = 20$, and $\Delta\theta_1 = 0.1, 0.5, 1.5$ radians (from left to right, corresponding respectively to hyperbolic distances $x_1 = 32, 35.2, 37.2$). The y -axis in the inset of (a) is in log-scale. The x -axis in (b) is binned into bins of size 0.1. The solid lines in the plots are the empirical distributions while the dashed black lines are the corresponding theoretical predictions. The empirical distributions are computed over all node pairs with $r_1 = 18 \pm 0.5, r'_1 = 20 \pm 0.5$ at the corresponding angular distance $\Delta\theta_1 \pm 0.05$. The empirical distributions in (b) are average distributions over 20 simulation runs.

3. Conditional PDF $f(x_2|x_1)$

Finally, let's consider $f(x_2|x_1)$. Since $x_1 \approx r_1 + r'_1 + 2 \ln \sin(\Delta\theta_1/2)$, we have:

$$\Delta\theta_1 \approx 2 \arcsin e^{\frac{1}{2}(x_1 - r_1 - r'_1)}. \quad (\text{D13})$$

Now, since we know how to compute $f(x_2|r_1, r'_1, \Delta\theta_1)$ (Eqs. (D10)-(D12)), we can write:

$$f(x_2|x_1) = \int \int f(x_2|r_1, r'_1, \Delta\theta_1) d\rho_1, \quad (\text{D14})$$

$$d\rho_1 \equiv \rho_1(r'_1) \rho_1(r_1) dr'_1 dr_1,$$

where $\Delta\theta_1$ is given in Eq. (D13) and $\rho_1(r_1)$ in Eq. (6). To be able to numerically evaluate Eq. (D14) we need to identify the limits of integration for the r_1, r'_1 variables and the corresponding integrands. Since Eqs. (D10)-(D12) consist of two-dimensional integrals, Eq. (D14) consists of four-dimensional integrals. This analysis is beyond the scope of this paper.

-
- [1] Dmitri Krioukov, Fragkiskos Papadopoulos, Amin Vahdat, and Marián Boguñá, "Curvature and temperature of complex networks," *Phys. Rev. E* **80**, 035101 (2009).
- [2] Dmitri Krioukov, Fragkiskos Papadopoulos, Maksim Kitsak, Amin Vahdat, and Marián Boguñá, "Hyperbolic geometry of complex networks," *Phys. Rev. E* **82**, 036106 (2010).
- [3] Fragkiskos Papadopoulos, Maksim Kitsak, M. Ángeles Serrano, Marián Boguñá, and Dmitri Krioukov, "Popularity versus similarity in growing networks," *Nature* **489**, 537 (2012).
- [4] Luca Gugelmann, Konstantinos Panagiotou, and Ueli Peter, "Random hyperbolic graphs: Degree sequence and clustering," in *Proc. of ICALP* (Springer, Berlin, Heidelberg, 2012) pp. 573–585.
- [5] Tobias Friedrich and Anton Krohmer, "Cliques in hyperbolic random graphs," in *Proc. of IEEE INFOCOM* (IEEE, Piscataway, NJ, 2015) pp. 1544–1552.
- [6] Tobias Friedrich and Anton Krohmer, "On the diameter of hyperbolic random graphs," in *Proc. of ICALP* (Springer, Berlin, Heidelberg, 2015) pp. 614–625.
- [7] Konstantin Zuev, Marián Boguñá, Ginestra Bianconi, and Dmitri Krioukov, "Emergence of soft communities from geometric preferential attachment," *Scientific Reports* **5**, 9421 (2015).
- [8] Mohammed Amin Abdullah, Nikolaos Fountoulakis, and Michel Bode, "Typical distances in a geometric model for complex networks," *Internet Mathematics* **1** (2017).
- [9] Nikolaos Fountoulakis and Tobias Muller, "Law of large numbers for the largest component in a hyperbolic model of complex networks," *Ann. Appl. Probab.* **28**, 607 (2018).
- [10] Marián Boguñá, Fragkiskos Papadopoulos, and Dmitri Krioukov, "Sustaining the Internet with hyperbolic mapping," *Nature communications* **1**, 62 (2010).
- [11] M. Ángeles Serrano, Marián Boguñá, and Francesc Sagués, "Uncovering the hidden geometry behind metabolic networks," *Mol. BioSyst.* **8**, 843 (2012).
- [12] Gregorio Alanis-Lobato, Pablo Mier, and Miguel Andrade-Navarro, "The latent geometry of the human protein interaction network," *Bioinformatics* **34**, 2826 (2018).
- [13] Antoine Allard and M. Ángeles Serrano, "Navigable maps of structural brain networks across species," arXiv:1801.06079 (2018).
- [14] Kaj-Kolja Kleineberg, Marián Boguñá, M. Ángeles Serrano, and Fragkiskos Papadopoulos, "Hidden geometric correlations in real multiplex networks," *Nature Physics* **12**, 1076 (2016).
- [15] Guillermo García-Pérez, Marián Boguñá, Antoine Allard, and M. Ángeles Serrano, "The hidden hyperbolic geometry of international trade: World trade atlas 1870–2013," *Scientific Reports* **6**, 33441 (2016).
- [16] Thomas Blasius, Tobias Friedrich, Anton Krohmer, and Soren Laue, "Efficient embedding of scale-free graphs in the hyperbolic plane," *IEEE/ACM Trans. Netw.* **26**, 920 (2018).
- [17] Fragkiskos Papadopoulos, Constantinos Psomas, and Dmitri Krioukov, "Network mapping by replaying hyperbolic growth," *IEEE/ACM Transactions on Networking* **23**, 198 (2015).
- [18] Fragkiskos Papadopoulos, Rodrigo Aldecoa, and Dmitri Krioukov, "Network geometry inference using common neighbors," *Phys. Rev. E* **92**, 022807 (2015).
- [19] V. Lehman, A. Gawande, B. Zhang, L. Zhang, R. Aldecoa, D. Krioukov, and L. Wang, "An experimental investigation of hyperbolic routing with a smart forwarding plane in NDN," in *Proc. of IEEE/ACM IWQoS* (2016) pp. 1–10.
- [20] Kaj-Kolja Kleineberg and Dirk Helbing, "Collective navigation of complex networks: Participatory greedy routing," *Scientific Reports* **7**, 2897 (2017).
- [21] Elisenda Ortiz, Michele Starnini, and M. Ángeles Serrano, "Navigability of temporal networks in hyperbolic space," *Scientific Reports* **7**, 15054 (2017).
- [22] Alessandro Muscoloni, Josephine Maria Thomas, Sara Ciucci, Ginestra Bianconi, and Carlo Vittorio Cannistraci, "Machine learning meets complex networks via coalescent embedding in the hyperbolic space," *Nature Communications* **8**, 1615 (2017).
- [23] Alessandro Muscoloni and Carlo Vittorio Cannistraci, "Minimum curvilinear automata with similarity attachment for network embedding and link prediction in the hyperbolic space," arXiv:1802.01183 (2018).
- [24] Mikko Kivelä, Alex Arenas, Marc Barthelemy, James P. Gleeson, Yamir Moreno, and Mason A. Porter, "Multilayer networks," *Journal of Complex Networks* **2**, 203 (2014).

- [25] S. Boccaletti, G. Bianconi, R. Criado, C. I. del Genio, J. Gómez-Gardeñes, M. Romance, I. Sendiña-Nadal, Z. Wang, and M. Zanin, “The structure and dynamics of multilayer networks,” *Physics Reports* **544**, 1 (2014).
- [26] Michael Szell, Renaud Lambiotte, and Stefan Thurner, “Multirelational organization of large-scale social networks in an online world,” *Proceedings of the National Academy of Sciences* **107**, 13636 (2010).
- [27] Peter J. Mucha, Thomas Richardson, Kevin Macon, Mason A. Porter, and Jukka-Pekka Onnela, “Community Structure in Time-Dependent, Multiscale, and Multiplex Networks,” *Science* **328**, 876 (2010).
- [28] Kimberly Claffy, Young Hyun, Ken Keys, Marina Fomenkov, and Dmitri Krioukov, “Internet Mapping: From Art to Science,” in *Proceedings of the 2009 Cybersecurity Applications & Technology Conference for Homeland Security, CATCH '09* (IEEE Computer Society, Washington, DC, USA, 2009) pp. 205–211.
- [29] Ed Bullmore and Olaf Sporns, “Complex brain networks: graph theoretical analysis of structural and functional systems,” *Nat Rev Neurosci* **10**, 186 (2009).
- [30] M. De Domenico, V. Nicosia, A. Arenas, and V. Latora, “Structural reducibility of multilayer networks,” *Nature Communications* **6**, 6864 (2015).
- [31] Kaj-Kolja Kleineberg, Lubos Buzna, Fragkiskos Papadopoulos, Marián Boguñá, and M. Ángeles Serrano, “Geometric correlations mitigate the extreme vulnerability of multiplex networks against targeted attacks,” *Phys. Rev. Lett.* **118**, 218301 (2017).
- [32] Roberta Amato, Albert Díaz-Guilera, and Kaj-Kolja Kleineberg, “Interplay between social influence and competitive strategical games in multiplex networks,” *Scientific Reports* **7**, 7087 (2017).
- [33] Kaj-Kolja Kleineberg and Dirk Helbing, “Topological enslavement in evolutionary games on correlated multiplex networks,” *New Journal of Physics* **20**, 053030 (2018).
- [34] Federico Battiston, Vincenzo Nicosia, and Vito Latora, “Structural measures for multiplex networks,” *Phys. Rev. E* **89**, 032804 (2014).
- [35] Ginestra Bianconi, “Statistical mechanics of multiplex networks: Entropy and overlap,” *Phys. Rev. E* **87**, 062806 (2013).
- [36] Davide Cellai, Eduardo López, Jie Zhou, James P. Gleeson, and Ginestra Bianconi, “Percolation in multiplex networks with overlap,” *Phys. Rev. E* **88**, 052811 (2013).
- [37] Yanqing Hu, Dong Zhou, Rui Zhang, Zhangang Han, Céline Rozenblat, and Shlomo Havlin, “Percolation of interdependent networks with intersimilarity,” *Phys. Rev. E* **88**, 052805 (2013).
- [38] M. Salehi, R. Sharma, M. Marzolla, M. Magnani, P. Siyari, and D. Montesi, “Spreading processes in multilayer networks,” *IEEE Transactions on Network Science and Engineering* **2**, 65 (2015).
- [39] Francis Bonahon, *Low-Dimensional Geometry* (AMS, Providence, 2009).
- [40] S. N. Dorogovtsev, *Lectures on Complex Networks* (Oxford University Press, Oxford, 2010).
- [41] “HyperMap-CN Software Package,” https://bitbucket.org/dk-lab/2015_code_hypermap.
- [42] “GMM-LP and conditional distances code,” <https://bitbucket.org/fpapadop/gmm-lp-and-conditional-distances-code/>.
- [43] F. Papadopoulos, C. Psomas, and D. Krioukov, “Replaying the Geometric Growth of Complex Networks and Application to the AS Internet,” *ACM SIGMETRICS Perform. Eval. Rev.* **40**, 104 (2012).
- [44] T. Saito and M. Rehmsmeier, “Precrec: fast and accurate precision-recall and ROC curve calculations in R,” *Bioinformatics* **33**, 145 (2017).
- [45] Arda Halu, Satyam Mukherjee, and Ginestra Bianconi, “Emergence of overlap in ensembles of spatial multiplexes and statistical mechanics of spatial interacting network ensembles,” *Phys. Rev. E* **89**, 012806 (2014).
- [46] Alessandro Muscoloni and Carlo Vittorio Cannistraci, “A nonuniform popularity-similarity optimization (nPSO) model to efficiently generate realistic complex networks with communities,” *New Journal of Physics* **20**, 052002 (2018).
- [47] Alessandro Muscoloni and Carlo Vittorio Cannistraci, “Leveraging the nonuniform PSO network model as a benchmark for performance evaluation in community detection and link prediction,” *New Journal of Physics* **20**, 063022 (2018).
- [48] A. Faqeeh, S. Osat, and F. Radicchi, “Characterizing the analogy between hyperbolic embedding and community structure of complex networks,” *Phys. Rev. Lett.* **121**, 098301 (2018).
- [49] Piero Mazzarisi, Paolo Barucca, Fabrizio Lillo, and Daniele Tantari, “A dynamic network model with persistent links and node-specific latent variables, with an application to the interbank market,” arXiv:1801.00185 (2018).
- [50] Ryuta Matsuno and Tsuyoshi Murata, “MELL: Effective embedding method for multiplex networks,” in *Companion Proceedings of the The Web Conference 2018, WWW '18* (International World Wide Web Conferences Steering Committee, Republic and Canton of Geneva, Switzerland, 2018) pp. 1261–1268.
- [51] “The IPv4 and IPv6 Topology Datasets,” http://www.caida.org/data/active/ipv4_routed_topology_aslinks_dataset.xml and https://www.caida.org/data/active/ipv6_allpref_topology_dataset.xml.
- [52] Chris Stark, Bobby-Joe Breikreutz, Teresa Reguly, Lorie Boucher, Ashton Breikreutz, and Mike Tyers, “BioGRID: a general repository for interaction datasets,” *Nucleic Acids Research* **34**, D535 (2006).
- [53] Beth L. Chen, David H. Hall, and Dmitri B. Chklovskii, “Wiring optimization can relate neuronal structure and function,” *Proceedings of the National Academy of Sciences of the United States of America* **103**, 4723 (2006).
- [54] Manlio De Domenico, Mason A. Porter, and Alex Arenas, “MuxViz: a tool for multilayer analysis and visualization of networks,” *Journal of Complex Networks* **3**, 159 (2015).
- [55] Tiago Simas, Mario Chavez, Pablo R. Rodriguez, and Albert Diaz-Guilera, “An algebraic topological method for multimodal brain networks comparison,” *Frontiers in Psychology* **6**, 904 (2015).
- [56] Manlio De Domenico, Andrea Lancichinetti, Alex Arenas, and Martin Rosvall, “Identifying modular flows on multilayer networks reveals highly overlapping organization in interconnected systems,” *Phys. Rev. X* **5**, 011027 (2015).
- [57] J. Coleman, E. Katz, and H. Menzel, “The diffusion of an Innovation among Physicians,” *Sociometry* **20**, 253 (1957).

- [58] M. Ángeles Serrano, Dmitri Krioukov, and Marián Boguñá, “Self-similarity of complex networks and hidden metric spaces,” *Phys. Rev. Lett.* **100**, 078701 (2008).
- [59] F. C. Leone, L. S. Nelson, and R. B. Nottingham, “The folded normal distribution,” *Technometrics* **3**, 543 (1961).
- [60] “Cuba open-source package,” <http://www.feynarts.de/cuba/>.
- [61] T. Hahn, “Cuba - a library for multidimensional numerical integration,” *Computer Physics Communications* **168**, 78 (2005).